Université de Neuchâtel
Institut de Microtechnique

Hydrogenated Microcrystalline Silicon Deposited by VHF-GD for Thin-Film Solar Cells

Thèse

Présentée à la Faculté de Sciences
pour obtenir le grade de docteur ès sciences
par

Pedro Torres

UFO Dissertation Band 352

Die Deutsche Bibliothek – CIP-Einheitsaufnahme

Torres, Pedro
Hydrogenated Microcrystalline Silicon Deposited by VHF-GD for Thin-Film Solar Cells / Pedro Torres. – 1. Aufl. – Allensbach : UFO, Atelier für Gestaltung und Verl., 1999
(UFO-Dissertation ; Bd. 352)
Zugl.: Neuchâtel, Univ., Diss., 1998
ISBN 3-930803-51-8

Dissertation der Universität Neuchâtel
Datum der mündlichen Prüfung: 28. August 1998
Referenten: Prof. Dr. A. Shah
Prof. Dr. J. Andreu
Prof. Dr. N. de Rooij
Dr. P. Seitz
Dr. A. A. Howling
Dr. H. Keppner

UFO Atelier für Gestaltung & Verlag GbR
Allensbach
Maus Druck & Medien GmbH, Konstanz
Erste Auflage 1999

ISBN 3-930803-51-8

IMPRIMATUR POUR LA THÈSE

Microcrystalline Silicon Deposited by VHF-GD for Thin Film Solar Cells

de M.Pedro Torres

UNIVERSITÉ DE NEUCHÂTEL

FACULTÉ DES SCIENCES

La Faculté des sciences de l'Université de Neuchâtel sur le rapport des membres du jury,

MM. A. Shah (directeur de thèse), N. De Rooij, H. Kepnner, J. Andreu Batallé (Barcelone), A. Howling (EPF Lausanne) et P. Seitz (CSEM, Zürich)

autorise l'impression de la présente thèse.

Neuchâtel, le 29 octobre 1998

Le doyen:

F. Stoeckli

Table of Contents

I. Introduction: The Thin-Film Silicon Solar Cell Challenge

Humankind has since ever increased its energy demands; it is the only living being of the "blue planet" that has overcome its natural fear of fire and to acquire, thus, an apparently unlimited access to energy. Quite a lot of time has past since this event and rudimentary combustion of wood in an open fire has indeed been significantly improved by tremendous technical advances over the past millenniums. At the verge of the 21 st century, it becomes, however, apparent, that unlimited growth is problematic; but that our so called "modern civilisation" relies completely on steadily increasing energy demands. Today's dominant energy resources (oil, coal, gas and nuclear power) are accompanied by severe problems related to air, water and surface pollution as well as the greenhouse effect. This is becoming unacceptable and unaffordable.

Photovoltaics (PV), the direct conversion of sunlight into electricity, basically has the potential to meet to some extend the rapidly growing demand for electricity with minimal environmental impact. The real challenge of photovoltaics lies in the reduction of the cost of solar cells while at the same time one should increase their conversion efficiencies. Only time will answer which of all the new photovoltaic technologies developed so far will survive in the long run in a more competitive energy market.

Silicon is the material of choice for the widespread application of solar modules for power generation, where large quantities of solar cells have to be set in the biosphere for decennials as silicon is non-toxic and already an abundant material in the earth's crust. Furthermore it is free of speculative actions which rise the prise of the feed stock.

Crystalline silicon (c-Si) solar cells could largely profit from the large know-how as accumulated by the IC-industry. In fact, silicon is the best known and studied material in the world. However, the cost reduction potential of the mature c-Si photovoltaic technology is almost fully accomplished: even though for now the market is dominated by panels incorporating c-Si solar cells, it is foreseeable that if production is further scaled up, problems with the crystalline silicon feed stock will arise. Low cost crystalline silicon wafers for the PV-industry come actually from the debris of the IC-industry and is not increasing at a sufficient pace to meet tomorrow's demand from the PV-industry.

On the other hand, an other form of silicon, namely hydrogenated amorphous silicon (a-Si:H), has inherently the potential to massively undercut the costs as set by panels assembled from individual c-Si solar cells. Hydrogenated amorphous silicon (a-Si:H) can advantageously be deposited by the plasma enhanced chemical vapour deposition (PECVD)

technique. PECVD has a large area capability (no need to assemble individual cells to a panel) and owing to the low deposition temperatures involved (lower than 250 °C) that hinder out diffusion of impurities deteriorating device performances it is possible to use inexpensive substrates. The development of a-Si:H has been a success story as far as production of thin film transistors (TFT) for flat panel screens as well as a photo conductor for xerographic application is concerned. However, a-Si:H had to proof that it can overcome the stigma of an inherently unstable material. The cell performance degrades at the beginning of prolonged light exposure before stabilising at 10 to 30 % below its initial conversion efficiency. However, for now, technological viable solutions have been found to render a-Si:H a more stable and reliable photovoltaic material. The policy of low-cost high efficiency a-Si:H solar cells has been followed up by our group by introducing the VHF-GD deposition technique. By extending the plasma excitation frequency from the standard 13.56 MHz to the VHF-range a higher deposition rate for a-Si:H without loss in cell efficiency has been demonstrated.

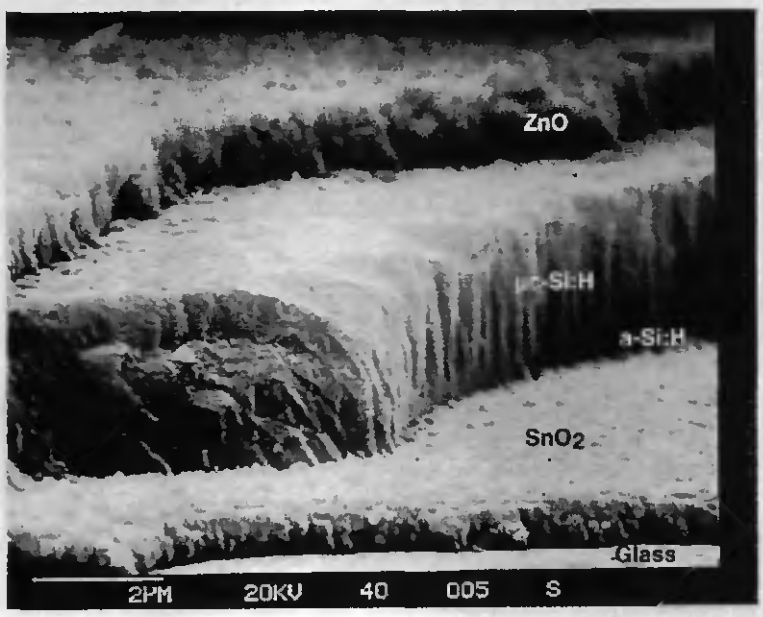

Fig. 1.1. Scanning Electron Micrograph of a Micromorph Thin-Film Silicon Solar Cell. Light is coming through the glass and SnO_2 layer (both transparent for visible light) and generates charge carriers in a-Si:H and μc-Si:H that are collected at the rear ZnO contact and front SnO_2 contact.

The global trend in photovoltaics to meet the low cost high efficiency dilemma can be called the thin-film silicon solar cell challenge. The challenge is manifold but lies principally in combining a priori incompatible technologies in one single device. Our contribution, developed at IMT and called the micromorph concept, is the combination of both amorphous and microcrystalline silicon. In this newly developed micromorph cell, a bottom microcrystalline silicon (μc-Si:H) solar cell is advantageously combined with an a-Si:H top cell in a monolithic tandem structure as can be seen in fig 1.1. Because of the different optical gaps, 1.7 eV for a-Si:H and 1.1 eV for μc-Si:H, a better use of the solar spectrum is possible. In fact, the spectral response of this micromorph tandem cell is extended to the red light compared with the spectral response of an a-Si:H because of the μc-Si:H bottom cell. Since μc-Si:H does not show a light induced degradation, the overall stability of the micromorph cell is also enhanced. Further, the newly developed μc-Si:H solar cell is full inline compatible with a-Si:H technology.

However, at the beginning of this work, some obvious problems of the microcrystalline cell hindered a faster development of this new photovoltaic material. This had also occured in the past: even though μc-Si:H had been already discovered in 1968 by Veprek [1], who also investigated the fundamnetal properties of this material in detail [2, 3], μc-Si:H was disregarded for quite a long time to be an active photovoltaic material.

The approach of the author of this work has thus been to develop μc-Si:H layers with the clear goal to be used in a photovoltaic device. Problems thereby encountered have been tried to be solved in such a way as to render this material as atractive as possible for a potential industrial application. The following outline of this work, that reflects its chronological development, shows that difficult to handle technologies were replaced by simpler ones that did not only lead to higher conversion efficiencies but also to significantly faster manufacturing times of single μc-Si:H solar cells.

Outline of this work

First section

For the purpose of this work a new Very High Frequency - Glow Discharge (VHF-GD) reactor was built by the author. This turned out to be very beneficial not only to learn basic vacuum technology but also to really understand and realise that the reactor and its handling has a direct impact on the quality of the intrinsic μc-Si:H layers that are required for PV-devices. Special emphasis was laid in obtaining an outgasing rate as low as possible to avoid oxygen contamination of the layers.

Additionally, in view of the later production of complete devices, the delicate to prepare p - doped μc-Si:H layers were reoptimised at our standard laboratory frequency of 70 MHz. The soft nature of VHF - plasmas as compared with standard 13.56 MHz plasmas is shown by obtaining epitaxial growth of such optimised p-layers on c-Si. Additionally, the plasma excitation frequency was extended to even higher frequencies of up to 130 MHz. Thereby, it was further evidenced that higher excitation frequencies not only allow to obtain higher deposition rates of high quality p-type μc-Si:H layers, but also that the deposition parameter window is substantially enlarged.

Second section

μc-Si:H layers are only useful for photovoltaic applications (in p-i-n or n-i-p diodes) when they can be tuned to be midgap, i.e. that their Fermi level lies at midgap. Before this work, this was achieved by adding small traces of diborane (in the ppm range) to the gas phase (silane and hydrogen) fed into the reactor. This so called "microdoping" approach was unfortunately a quite delicate technology to master.

By controlling as far as possible the oxygen contamination, it turned out that device grade μc-Si:H can be obtained without any microdoping. In our work this was achieved by controlling impurities coming from the outgasing of the reactor and by purifying the source gas by a getter-based purifier. The impact of this approach has not only been to replace the microdoping approach but has also resulted in significantly enhanced conversion efficiencies of μc-Si:H solar cells.

Third section

The "purifier approach" opened the door for an efficient search for new deposition conditions to overcome the ususally low deposition rate of μc-Si:H.

In this section, we present results of attempts to significantly enhance the deposition rate of our intrinsic μc-Si:H silicon. For use in solar cells, a thickness of about 3.5 μm of μc-Si:H is required in order to absorb enough sunlight. The usual deposition rates, even with the inherently faster VHF-GD deposition technique, were around 1 Å/s. With such a low deposition technique, the main goal of working towards a low-cost high-efficiency solar cell would have been jeopardised by a net deposition time of 10 h for this intrinsic layer.

By systematic increasing of both, the silane concentration and the VHF-power level, a 10 fold increase in deposition rate has been achieved. Such layers have also successfully been integrated into μc-Si:H solar cells. We could also bring to evidence, that if the excitation frequency is high enough, the detrimental ion bombardment for the layer quality can be maintained low enough even when the VHF-power is substantially increased.

II. The VHF - GD Deposition Technique

2.1. Introduction

There are several known possibilities how to deposit thin silicon films from the gas phase directly on a substrate. One way is to provide high enough thermal energy for the dissociation of the source gas. This is done in the widely used Chemical Vapour Deposition technique (CVD) where the substrate is maintained at relatively high temperatures. The deposition of the so-called "polysilicon" requires in general temperatures in excess of 600 °C [4] and by that requires temperature resistant substrates. The risk of autodoping (doping by impurities present in the system) at such high temperatures is high.

If the dissociation of the source gas is enhanced by a plasma discharge, much lower process temperatures (typically below 300 °C) for the deposition of silicon films are necessary; this technique is called plasma enhanced chemical vapour deposition (PECVD). Such low temperatures allow a larger choice of different substrate materials. The deposition process by PECVD can be tuned in such a way that either amorpbous silicon or microcrystalline silicon may be obtained.

To avoid confusion we will denominate in this work as polycrystalline silicon the material deposited by CVD and as hydrogentaed microcrystalline silicon (μc-Si:H) the films deposited by PECVD. Note that these names are not related to the grain size since both, polycrystalline and microcrystalline silicon can have the same grain size (50-1000 Å).

In the case of silicon nitride, just to mention another example, the process temperature is reduced from 700-800 °C necessary for CVD down to 250-350 °C when using PECVD. Such low temperatures are the only way to use this material with its excellent passivation properties over the final device metalisation in VLSI technology [4].

The type of plasmas used in PECVD are called "cold plasmas". The plasma is not in thermal equilibrium, i.e. the energy of the ions and free electrons is not equal. Most of the RF-power is actually picked up by the electrons due to their lower mass as compared to the reminder ions. The dissociation of the source gas is substantially enhanced by impact ionisation caused by electrons that have gained enough kinetic energy from the RF-field.

The flux of neutral radicals onto the substrate leads to the growth of the film whereas atomic hydrogen etches the growing film when hydrogen-dilution is used as in the case of μc-Si:H. As a result, depending on the plasma conditions, different growth conditions can result. Thus PECVD grown silicon thin films have substantially different properties than those grown by CVD.

2.2. Particularities of VHF - GD

Standard PECVD is performed at a frequency of 13.56 MHz. The choice of this particular frequency comes from legislative restrictions concerning the power emitted at attributed telecommunication frequency bands (e.g. the FM - band lies at 88-108 MHz).

However the excitation frequency has been shown to be considered as a key plasma parameter deserving a keen investigation. Pioneering work was done in our group to extend the plasma excitation frequencies to the very high frequency band: Curtins et al. reported in 1987 [5] a remarkable increase of the deposition rate of a-Si:H together with good material quality achieved by increasing the plasma excitation frequency from the standard 13.56 MHz up to 70 MHz.

Hereafter we will give a short summary of differences that have been found between standard PECVD and VHF-GD with emphasis on relevant features for μc-Si:H growth. Thereafter the VHF reactor that was built for this study is described, including the particular contributions of this work that further demonstrate how VHF-GD is well suited for the growth of μc-Si:H.

Experimentally it has been observed by several authors, that the deposition rate of a-Si:H increases by increasing the plasma excitation frequency, maintaining other process control parameters (pressure, gas flow, RF-power, reactor geometry) effectively constant [5-7]. Several factors controlling this enhanced deposition rate have been elucidated. Recently it has also become more and more evident that some of the factors which lead to higher deposition rates for a-Si:H are also playing an important role in the growth mechanism of μc-Si:H.

It has been observed that at higher excitation frequencies one bas:

- a higher electron density (and by that higher dissociation rates)
- the RF-power is dissipated rather to the bulk than to the sheath (a reduced sheath thickness is observed)
- a reduced sheath potential between the plasma and the substrate leads to lower peak ion energies with an enhanced flow of (low energy) ions to the substrate. By that ion bombardment enhanced surface reactions or desorption of chemisorbed species and reaction of radicals that contribute to the films growth, is enhanced.

As shown in fig. 2.1, Heintze et al. [7] measured an enhanced ion flux on the growth surface at higher frequencies. This is related to the changes in the bulk plasma and the sheath. They suggested that the enhanced ion flow to the growth surface could well be the growth-

rate controlling mechanism in the deposition of a-Si:H material due to an increased surface reactivity of the film precursors.

The reduced peak ion energy also observed (see fig. 2.1.) is a direct consequence of the reduced sheath potential and it has been proposed that this might be the reason why VHF-plasmas favour μc-Si:H growth [8].

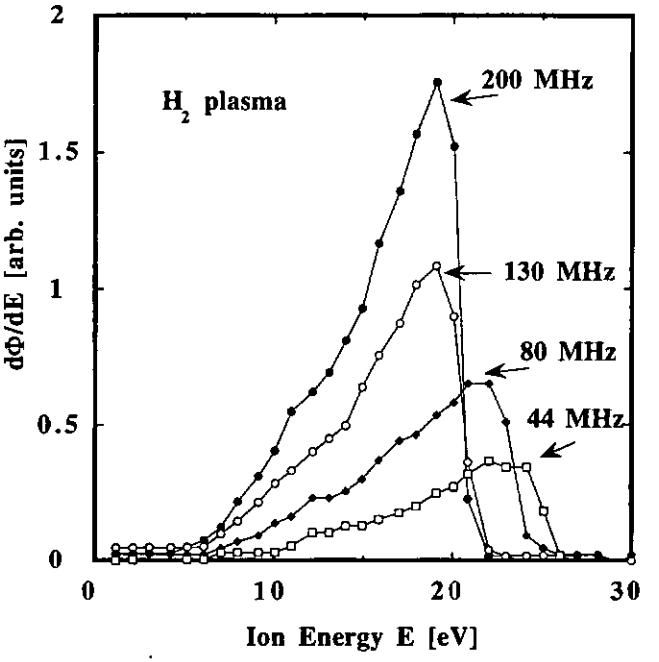

Fig. 2.1. Ion energy distribution of positive ions on the substrate, measured in an H_2 plasma: The flux of ions is roughly proportional to the excitation frequency. At the same time, we observe a decrease in the maximum ion energy up to 130 MHz. Data taken from M. Heintze and R. Zedlitz [7].

2.3. The VHF-GD Deposition System

Parts and components designed for operation at the standard 13.56 MHz excitation frequency are easily available on the market. However, deposition systems operating at higher excitation frequency are not (yet) commercialised. Here, at IMT, we built up our own deposition reactors with VHF capability. This research reactors are quite flexible for research purposes and are steadily improved. Apart from getting better experience in vacuum

technology, this approacb of building up our own deposition reactors allows us to understand better how the deposition processes are influenced by the "tool", i.e. the deposition reactor (and vice versa).

2.3.1 The deposition system

Fig. 2.2. shows a schematical sketch of the parallel-plate VHF-GD reactor that was built-up for this work. The reactor vessel consists of stainless steel and is basically a sphere with two double crosses for the connections to other vacuum components (see fig. 2.3.). All the direct connections to the reactor are provided by the Conflat system (CF) which allows to handle high bake-out temperatures (sealing is provided by a copper gasket) and ensures low leak values.

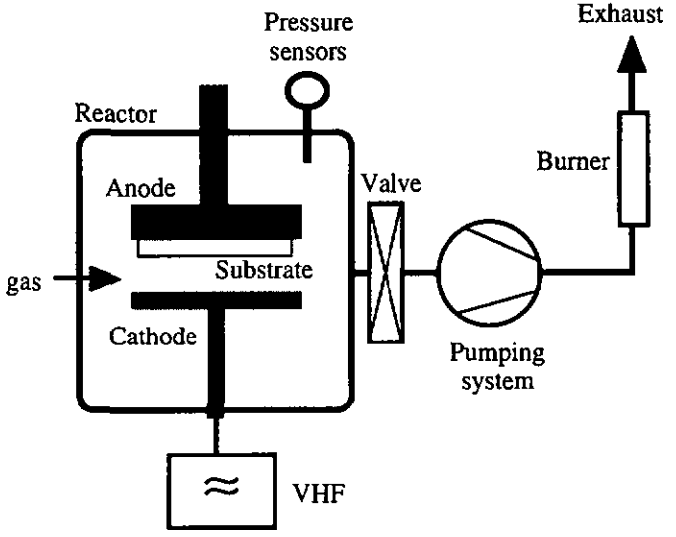

Fig. 2.2. Schematical representation of the VHF-GD deposition system with its major components.

The bigger double cross (CF 200) accommodates both electrodes and allows a close connection to the pumping system. Accessibility to the inside of the reactor is provided by a front door. A small window integrated in the door allows a direct observation of the plasma. The reactor system is further connected to a load-lock system (see fig. 2.3.) in order to minimise pump down cycles and to avoid contamination of the system.

Both electrodes have a heating capability. Charging of the substrate to the upper grounded electrode (anode) is done by means of a substrate holder. Substrates up to sizes of 8.3×8.3 cm^2 can easily be fixed on this substrate holder.

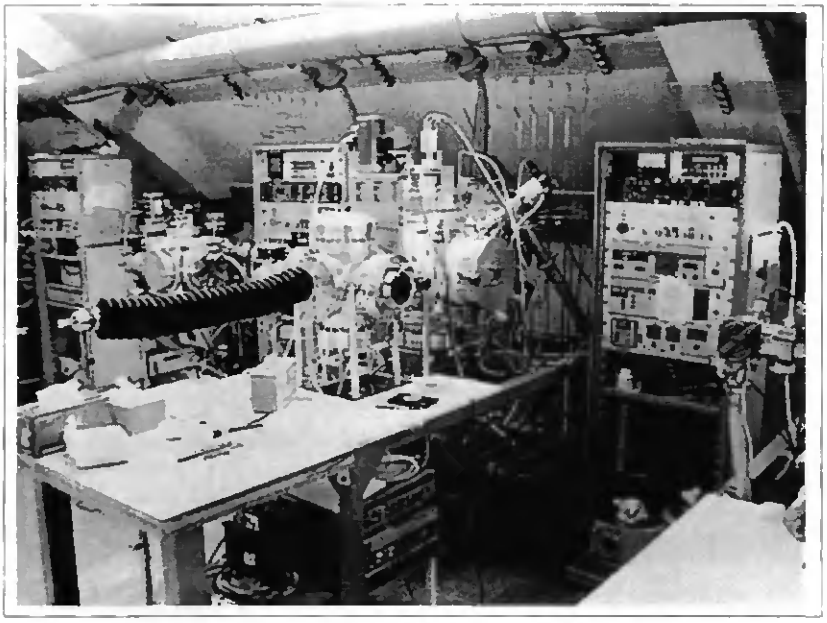

Fig. 2.3. Picture of the VHF-GD deposition system. Every deposition system in the laboratory has its own control rack and operates independently from the other reactors.

The powered lower electrode (cathode) is connected to the VHF-source by means of an impedance matching network which is called for simplicity "matchbox". The output impedance of the power amplifier (usually 50 Ω) is manually adjusted to the impedance of the reactor. This matching procedure is monitored by a standing-wave-ratio (SWR) power meter inserted in the coaxial line just before of the "matchbox". The SWR power meter measures thereby the forwarded as well as the reflected power; during the deposition process one has to minimise the reflected power. Excellent matching capability is achieved in a wide VHF-frequency range of 55 - 180 MHz. Ignition of the plasma is easily achieved by a high voltage spark from a commercial gas flame ignitor (piezoelectric quartz) that is applied to an electrical feed through of the chamber.

The reactor walls have a heating facility to bake out the system to achieve a good base pressure. Furthermore, a water cooling circuit allows to maintain the chamber walls at low temperatures, even with heated electrodes (250 °C) and during the process when the pressure

in the chamber is high enough to heat up the walls through convection. Because the outgasing rate depends mostly on the temperature of the chamber walls, this water cooling circuit ensures a higher stability of the deposition process. By this way contamination of the films related to the outgasing rate remains constant and controllable during the time of deposition. Further, the system has been equipped with a load-lock charging facility to mioimise pump-down cycles.

Precise control of the flow of gases is provided by flowmeters. The available gases were argon (Ar), hydrogen (H_2), silane (SiH_4), methane (CH_4), carbon dioxide (CO_2), nitrogeo (N_2), diborane (B_2H_6) and phospine (PH_3). The latter two are diluted respectively at 500 and 1000 ppm into hydrogen. An optional gas purifier allows to reduce oxygen contaminants in the source gas. Oxygen contamination of the source gas is due to the outgasing in the relatively long gas lines in the laboratory but is also originally contained in the gas bottles.

The pressure of the chamber is monitored by a Pirani and a Penning gauge. During the process, the pressure is controlled by a baratron gauge (capacitive manometer) which has a higher precision at the usual pressure range of the process (typically 0.1 to 1 mbar). The process pressure is controlled by a positionable valve which is controlled electronically and is situated between the chamber and the pumping system. To avoid burning of the plasma between the powered RF-plate and the border of the electrode a shield is installed as described in detail in earlier work of our group [9].

The pumping system consists of a process compatible turbomolecular pump backed by a double stage oil-sealed mechanical rotary pump (primary pump). There is no need to switch between a high vacuum pump and a process pump. During the deposition process, nitrogen is admitted by a "gas ballast" facility into the primary pump to avoid coodensation of vapour and to dilute the process gas. The extracted process gas is then decomposed in a burner at about 650 °C before reaching the environment.

2.3.2 Characterisation and operation of the deposition system

All deposition temperatures indicated in this work are effective substrate temperatures as obtained by calibrating the substrate temperature. Calibration of the temperature was done by measuring the effective substrate temperature for realistic gas pressures as used for the deposition process in order to take in account the effect of substrate heating by convectioo of the gas.

Gas flows were calibrated under isothermal conditions. The whole system (with the electrodes) was cooled down to room temperature. Calibration was done by the pressure rise method. Once the gas flow as controlled by the flowmeter is stable, the chamber is isolated from the pumping system and the pressure rise Δp (in mbar) is measured for a given time

interval Δt (in sec). Knowing the volume of the chamber (36 l), the gas flow ϕ in standard cubic centimeters (sccm) can be calculated as:

$$\text{Gas flow:} \qquad \phi(\text{sccm}) = 60 \cdot V \cdot (\Delta p/\Delta t) \qquad (2.1.)$$

Similarly, the outgasing rate of the reactor is also measured by isolation of the whole reactor and measuring the pressure rise for a known time interval. This evaluation procedure is done particularly just before the deposition of the intrinsic layers as will be discussed later. The outgasing rate is calculated as:

$$\text{Outgasing rate} \qquad \phi(\text{mbar l / sec}) = V \cdot (\Delta p/\Delta t) \qquad (2.2.)$$

As shown in several publications special care has to be taken, to specify the applied VHF-power to the plasma. Non negligible losses render the effective applied VHF-plasma power in some cases significantly lower. A method to evaluate the effective power applied to the plasma which has been used in our experiments is the subtractive method [6, 10]. It can be shown, that at a constant peak to peak value the power applied to the plasma equals to:

$$\text{Effective plasma power} \qquad P_{eff} = P_{appl} - P_{loss} \qquad (2.3.)$$

This graphical method allows to access the effective plasma power (Peff) by substracting from the applied plasma power (Pappl) the network losses (Ploss). Network losses are measured under vacuum conditions. A more detailed desciption of this evaluation method is given in section 4.3.1.

2.3.3 Substrates

In the following, we will mention case by case which substrate was used. In fact, depending on the measurement technique we plan to apply for the characterisatinn of the µc-Si:H films, different substrates bave been used:

-Sodium free glass (for optical and electrical characterisation, X-Ray)
-wafers (for IR measurement, epitaxy)
-SnO2 coated glass from Asahi (for p-i-n or n-i-p devices)
-Aluminium or stainless steel sheets coated with sputtered ZnO/Ag (for n-i-p devices)

All these substrates can be loaded on the same electrode, and thus µc-Si:H films can be deposited in the same run on different substrates.

2.4. Two studies illustrating advantages of VHF-GD for crystalline silicon growth

Hereafter we will give results of two studies that illustrate that the VHF-GD deposition technique is particularly well suited for the growth of the crystalline phase of silicon.

In the first section, we show that an increase of the excitation frequency results in an enlarged parameter space for the deposition of thin p-type μc-Si:H layers. Doping of such layers is achieved by adding diborane into the gas phase. However, diborane is known to hinder the crystalline nucleation. Here we will show that thanks to the higher employed excitation frequency higher quantities of diborane can be applied to the gas phase without preventing crystalline nucleation.

In the second section it is shown that such a highly diborane doped layer, as optimised on glass, can even grow epitaxially if a crystalline wafer is used as a substrate. This result is remarkable w.r.t. the low deposition temperature of only 170°C that is used here and illustrates, once again, the "soft nature" of VHF-GD: We have proposed that the maximum kinetic energy of the impinging ions is below the energy level to create defects in the Si crystal [11].

2.4.1. Enlarged parameter space for thin p-type μc-Si:H layers

In this chapter new results on thin p-type μc-Si:H films [12] deposited at low temperatures (170 °C) by the VHF-GD are presented.

Doped μc-Si:H layers are excellent contact layers for photovoltaic applications due to their higher doping capability and conductivity as compared to amorphous silicon. However, the major drawback of growing very thin boron doped μc-Si:H layers is that it is technologically quite a delicate task to find the appropriate parameters to avoid a phase transition to a-Si:H for very thin layers. One has to ensure that the layer is indeed microcrystalline. This morphological requirement is usually achieved by highly diluting silane in hydrogen. Standard 13.56 PECVD requires, in general, dilution ratios higher than 1 % SiH_4/total gas flow. On the other hand, the VHF-GD technique allows for lower dilution ratios, i.e. of 5 % SiH4/total gas flow, for μc-Si:H growth [13] and even beyond under high VHF-power conditions as will be shown in section 4. However, earlier studies on p-type μc-Si:H have clearly shown [14, 15] that doping has to be carefully adjusted: the optimum diborane doping ratio (B_2H_6/SiH_4) for highly conductive films has to be determined empirically: on one hand, enough doping is needed to push the Fermi level close to the valence band, on the other hand, a too high doping will result in the amorphisation of the layers [16-18].

Earlier studies [13, 19] have shown that VHF-conditions are favourable for microcrystalline growth. The better growth of μc-Si:H at higher plasma excitation frequencies motivated us to further increase the excitation frequency in order to try to obtain even higher conductivities. So far, comparative excitation frequency studies for μc-Si:H growth have been carried out only on n-type μc-Si:H [19].

The films in this study were deposited on AF45 glass from Schott at plasma excitation frequencies of 70, 100 and 130 MHz. To avoid cross-contamination from outgasing, the reactor chamber walls were heated ovemight, leading thus, to a base pressure of $5 \cdot 10^{-8}$ mbar at room temperature. To achieve high reproducibility, all layers were deposited with the same chamber history. The employed gases were SiH_4, H_2 and B_2H_6 diluted at 500 ppm in H_2. Gas pressure was kept constant at 0.4 mbar and dilution level of silane was 1.5 % over a total gas flow of 100 sccm. The effective VHF-power, determined by the subtractive method was kept constant at approximately 3.5 W. This corresponds to setpoint values of 4, 5 and 9 W for the respective excitation frequencies of 70, 100 and 130 MHz. One can observe from this measurements that the power coupling efficiency becomes worse at higher excitation frequencies.

As a monitor of the doping efficiency, the value of the room temperature dark conductivity (σ_d) under an N_2 atmosphere at 10 mbar after a standard temperature annealing step up to 150 °C was chosen. Optimal doping was chosen when σ_d reaches a maximum value.

The layer thickness was kept constant at around 400 ± 100 Å as measured by α-step (profilometry) for optimisation of the boron doping experiment. This was chosen in order to avoid errors due to the strong thickness effect on σ_d, as observed for very thin layers [20]. In order to maximise σ_d, a doping-study was carried out for the different plasma excitation frequencies: 70, 100 and 130 MHz. From fig. 2.6. it is obvious that the doping range for highly conductive p - type μc-Si:H films is broadened when the plasma excitation frequency is increased. From this result we deduce, that higher excitation frequencies favour the growth of p - type μc-Si:H layers. This effect is also interesting from the point of view of plasma physics, since it provides further experimental evidence that the VHF-GD technique at high plasma excitation frequencies is indeed an appropriate tool for the growth of μc-Si:H. Here, we observe that even a higher amount of diborane in the gas phase ratio does not hinder crystalline nucleation if one moves to higher plasma excitation frequencies.

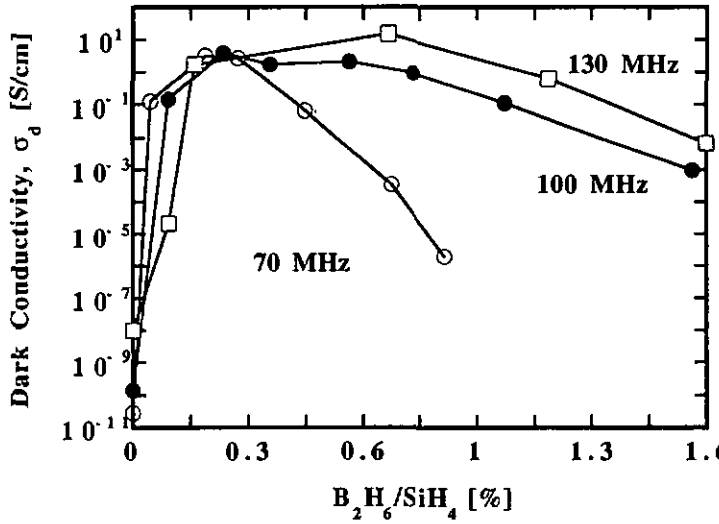

Fig. 2.6. Room temperature dark conductivity as a function of diborane doping for three different rf-plasma excitation frequencies. Film thickness is nominally 400 Å.

From fig. 2.6. we deduce that the optimal diborane doping ratio (B_2H_6/SiH_4) for the 70 MHz series is about 0.2 % and that this optimum is shifted to a higher value of about 0.7 % for the 130 MHz series. To compare this 130 MHz p - type films with an earlier study done at 70 MHz [14], we deposited a thickness series at 0.7 % B_2H_6 doping as assumed to be optimal for 130 MHz (fig. 2.6.). It is well-known that for thicknesses under a critical value, the dark conductivity σ_d will drop substantially [20].

In fig. 2.7. we compare the 130 MHz series with a 70 MHz series already published [14] which was deposited in an equivalent reactor and under similar conditions. It is surprising that even under such different growth conditions the films have the same thickness dependency of the electrical properties. In fig. 2.8. we show the optical transmission of the 130 MHz thickness series. Although the highly conductive films (d > 180 Å) show considerable absorption in the visible range, but the appropriate thickness, e.g. for a window layer in a solar cell, has to be worked out in the device itself, as the nucleation behaviour can strongly depend on the underlying substrate (see also section 2.4.2).

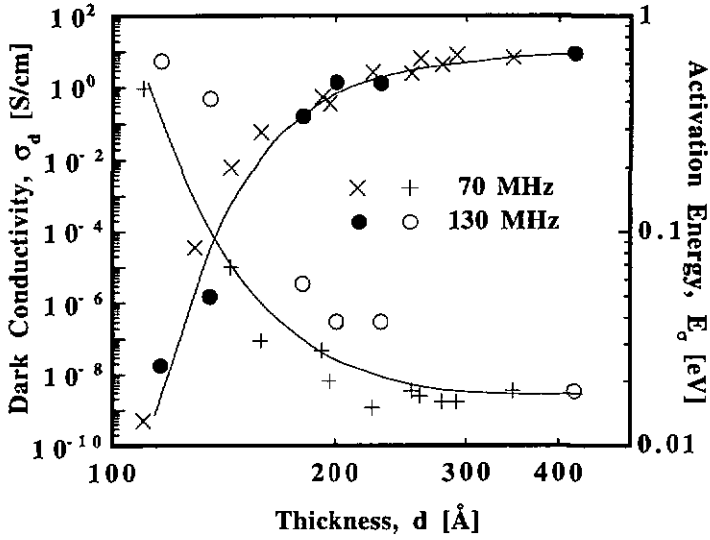

Fig. 2.7. Room temperature dark conductivity and dark conductivity activation energy, as a function of film thickness. Note that the 70 MHz series are taken from R. Flückiger et al. [20, 21] and were deposited in an equivalent reactor under similar conditions.

The deposition rate of boron-doped films depends strongly on the B_2H_6/SiH_4 gas phase ratio. To compare the deposition rates of highly conductive films obtained by different plasma excitation frequencies, we kept the gas phase doping ratio at the constant values of 0.2 % B_2H_6 / SiH_4; the result is shown in fig. 2.8. For comparison, the 130 MHz film with optimal doping of 0.7 % is also shown in the same figure. We see that an increase in excitation frequency results in higher deposition rates: the deposition rate is doubled by increasing the excitation frequency from 70 to 130 MHz. An even higher deposition rate is observed when increasing the diborane doping ratio. Note that this increased deposition rate does not affect the film quality in terms of electrical conductivity as seen in fig. 2.7, provided that the excitation frequency is high enough.

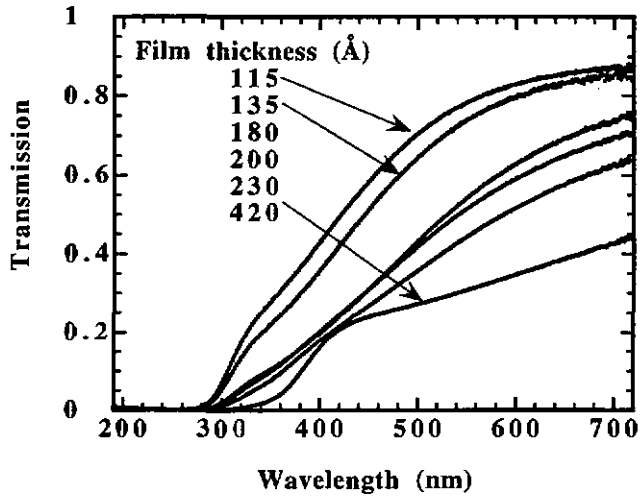

Fig. 2.8. Optical transmission of p-type layers deposited at a plasma excitation frequency of 130 MHz for a set of layer thicknesses as shown in fig. 2.7.

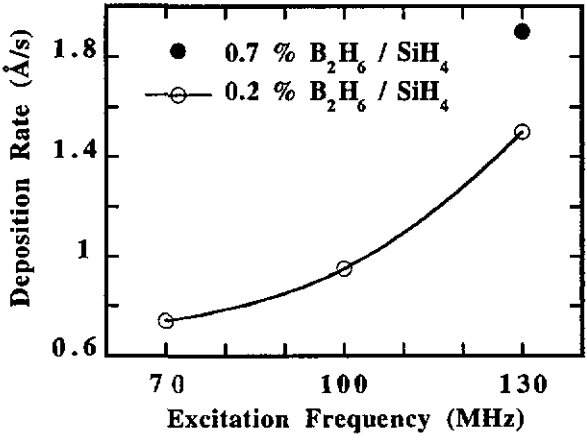

Fig. 2.9. Deposition rates of diborane doped microcrystalline silicon films deposited on glass at several plasma excitation frequencies. Further doping increases the deposition rate. In the case of the layer grown at 130 MHz, 0.7 % corresponds to the optimum amount of doping (maximum of σ_d at room temperature).

Starting from previously published results on p - type μc-Si:H, deposited at an excitation frequency of 70 MHz, where the VHF-GD method had already been shown to give excellent layers w.r.t conductivity and activation energy, we have extended the plasma excitation frequencies to even higher frequencies of 100 and 130 MHz. Thereby, we found that the parameter range for the diborane gas phase doping ratio is substantially enlarged. This effect supports earlier findings that higher plasma excitation frequencies lead to higher crystallinity and higher deposition rates of the μc-Si:H films. Note, that 130 MHz has not to be considered as an upper limit as in a recent work excellent p-type μc-Si:H has been demonstrated at a single excitation frequency of 170 MHz [22]. Indeed, they found a similar result, that is a broader doping regime for p-type μc-Si:H.

As an outlook, this larger parameter space at the higher plasma excitation frequency of 130 MHz could probably also facilitate the growth of boron-doped μc:Si,C:H layers, i.e. of silicon - carbon alloy. There, methane used in the gas phase is also known to hinder nucleation [15]. Higher plasma excitation frequencies may thus favour the growth of SiC - crystallites; in a similar way, Hamakawa et al. claim to obtain SiC crystallites when using the ECR - process at 2.45 GHz [23]: The enlarged parameter space at higher frequencies demonstrated here may possibly constitute a tool to overcome this limitation.

In section 4, where we will show how to obtain higher deposition rates for undoped μc-Si:H, we will make use of this here found larger parameter space at higher excitation frequencies.

2.4.2. Epitaxial growth at a very low temperature of 170 °C

Doped epitaxial layers deposited at very low temperatures are generally interesting for ULSI technology, opto-electronics in TFT's, as well as for crystalline pn solar cells [24, 25]. In this case, abrupt junctions can be built "externally" without interdiffusion of dopants occuring during the high temperature process of doping by diffusion. Moreover, low temperature epitaxial growth can reduce auto-doping, wafer warpage and system design cost. The results presented in this section have already been published elsewhere [26].

So far, a variety of techniques have been employed to grow silicon epitaxial layers, at rather low temperatures; some examples are: the use of chloride [27] and halide [28] gases (note that these gases are problematic from an environmental point of view), molecular beam epitaxy [29], synchrotron-radiation photochemical vapour deposition [30], dc magnetron sputtering [31] and, also, a modified rf-dc magnetron sputtering method which lowers the kinetic energy of the particle bombardment [32]. Early work of Townsend et al. [33] in 1972, and the work reported by Comfort et al. [34] in 1987 already used the inherent advantages of PECVD but at the rather high temperatures of about 800 °C. With this technique, in situ cleaning is easy to perform and the plasma provides the (non-thermal) energy during the

epitaxial growth. By then, Veprek [35] raised the question, whether epitaxial Si films could be grown by PECVD at very low temperatures with sufficiently high deposition rate and film quality. To reach this goal, one approach within PECVD is to keep the plasma, which is "breeding" the radicals, away from the growing epitaxial layer, in order to avoid the creation of crystal defects by impact of high energy ions. This can be done e.g. by electron cyclotron resonance PECVD [36, 37], by remote plasma CVD [38] or by controlling the ion energy with a mesh inserted between the plasma and the substrate [39]. Notwithstanding, it has been shown that even standard PECVD permits the growth of high quality undoped epitaxial layers as shown by Tsai et al. [40] and by Chen et al. [41, 42]. Standard PECVD has additional advantages such as capability for large-area deposition, low cost and simple realisation of batch-wafer processing.

However, all these low temperature epitaxial layers produced by Tsai et al. [40] and by Chen et al. [41, 42] were undoped. In order to epitaxially grow p - doped layers, an additional difficulty has to be overcome, namely the tendency of amorphisation of the material when high amounts of boron is added to the gas phase. To address this problem, we made use of the strong analogy that exists between epitaxial silicon growth on wafers and the growth of hydrogenated microcrystalline silicon (μc-Si:H) films on glass. The favourable growth conditions of μc-Si:H deposited by VHF-GD are understandable from the results of plasma investigations: it has been found [43], that an increase of the excitation frequency results in a decrease of the average ion energy and in a bigher ion flux to the growing substrate. It is supposed that an enhanced ion flux with moderate ion energy gives rise to an increased surface mobility of ad-atoms near the growing surface, thereby favouring the growth of crystallites. This effect will be favourable for both the growth of μc-Si:H layers and of epitaxial silicon layers.

In this chapter we report on the growth of strongly boron-doped epitaxial and μc-Si:H layers by the VHF-GD technique at temperatures as low as 170 °C. These results are of interest both for the actual growth of epitaxial films and, also scientifically, to obtain a better general understanding of the initial nucleation of silicon crystallites on different substrates [see e.g. 23] including crystalline silicon.

Basically, we investigated two types of diborane-doped layers: In a first step, boron doped μc-Si:H layers were deposited on glass in order to optimise the diborane doping ratio as the layer quality could be easily monitored by looking at the dark conductivity σ_d. In a second step, using these optimised doping parameters, epitaxial layers were deposited on crystalline wafers, where we restricted the analysis to cross-sectional high resolution electron micrographs (HREM) obtained by transmission electron microscopy (TEM).

This two step proceeding was necessary as the optimal diborane doping ratio (B_2H_6/SiH_4) to obtain highly doped films has to be determined empirically since, on the one

hand, enough doping is needed to push the Fermi level close to the valence band, but, on the other hand, too higb doping results in an amorphisation of the layers [16, 17].

This optimisation process of the boron doping for a given frequency (70 MHz) and layer thickness (400 Å) was already described in detail in the previous chapter. The result thereby obtained is shown in fig. 2.10, where the dark conductivity is plotted as a function of diborane doping ratio: The optimum doping ratio is about 0.25 % of diborane in silane, for the chosen parameters and at a plasma excitation frequency of 70 MHz.

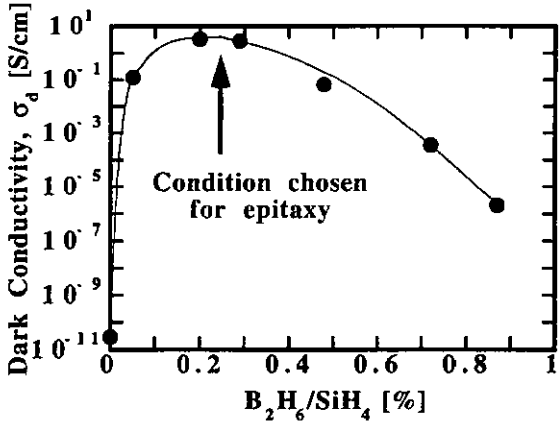

Fig. 2.10. Room temperature dark conductivity versus diborane doping ratio. The added line is for guiding the eyes.

Once the optimal set of parameters to grow μc-Si on glass was found, it was applied to the deposition on c-Si wafers. Employed substrates were p-type CZ-grown c-Si of <100> orientation with a resistivity of 5-7 Ωcm. The standard procedure before loading the substrates was either a rinse with deionised (DI) water or a HF-dip and then drying with a N_2 jet. The silicon substrate surface was exposed to air for about 5 min. while loading into the reactor after the cleaning procedure. Note, that the wafers did not receive any further ex-situ cleaning and that they were used as sold by the manufacturer. Additionally, the deposition system is not in a clean room environment.

Prior to deposition, the water-rinsed substrates received successively for 10, 20 and 5 minutes, respectively, the following in-situ treatments: argon plasma, hydrogen flushing at 0.95 mbar and hydrogen plasma. The HF-dipped substrates just received an in-situ hydrogen flushing. During all these pre-treatment steps, the substrates were already kept at the fixed deposition temperature of 170 °C. In the following we will show that the sample preparation has a crucial effect on the growing layer.

The substrate which just received a DI-water rinse is still covered with a native oxide layer and hence no ordered structure is given to the ongrowing layer. This can be seen in Fig. 2.11a, where a dark line (the oxide?) between the wafer and the grown layer can be seen. Small crystallites can be seen within the layer, as is usual for μc-Si:H, but by no way, we are dealing with epitaxial growth, since the structure of the wafer is completely screened by the native oxide.

The wafer which received several plasma pre-treatment steps can be seen in fig. 11b together with the deposited layer. Owing to the plasma attack, the oxide covering the substrate has been partially etched away. However, no effect on the initial nucleation of the deposited layer can be seen if we compare with the previous fig. 11a where the oxide layer was not attacked at all. From this experiment it is, thus, unclear whether a plasma etching step is able to remove the oxide layer in such a way, that subsequent epitaxial growth would still be possible, i.e. without causing lattice damage. This question still remains open.

In fig. 11c, epitaxial growth is clearly observable. Whilst depositing the ongrowing layer, steps on the crystalline surface are encountered, favouring, thus, crystalline growth. Here, the native oxide of the wafer has been removed by the applied HF-dip. It is evident that the same orientation persists from the bottom to the top of the epitaxially grown layer. The interface in this case looks atomically flat, however, stacking faults can be seen. The epitaxial layer has a thickness of 375 Å with a corresponding deposition rate of 0.74 Å/sec.

In conclusion we have shown for the first time that epitaxial growth of boron-doped crystalline silicon can be performed using the VHF-GD technique at temperatures as low as 170 °C. We propose that at VHF plasma excitation frequencies, an increased ion flux to the surface of the substrate gives rise to an enhanced surface mobility even at very low substrate temperatures, i.e. the surface mobility might in our case be mainly controlled by the plasma. Furthermore, the reduced peak ion energy in VHF plasmas allows for deposition conditions that do not induce too many lattice defects in the orienting substrate and within the growing layer [11].

The VHF-GD process bears, hence, the potential to fabricate crystalline silicon pn solar cells below 200 °C by using either a single-junction approach (as already demonstrated by the author [25, 44]) or a multijunction approach [45]. As the evidence of low temperature epitaxial growth is given in this thesis for boron-doped silicon, it should also be possible to grow epitaxial phosphorous-doped layers with this same technique, because crystallisation is less difficult in the case of phosphorous doping [18]. Additional advantages like large-area deposition, low cost and easy batch-wafer processing capability are inherent in the technique used here.

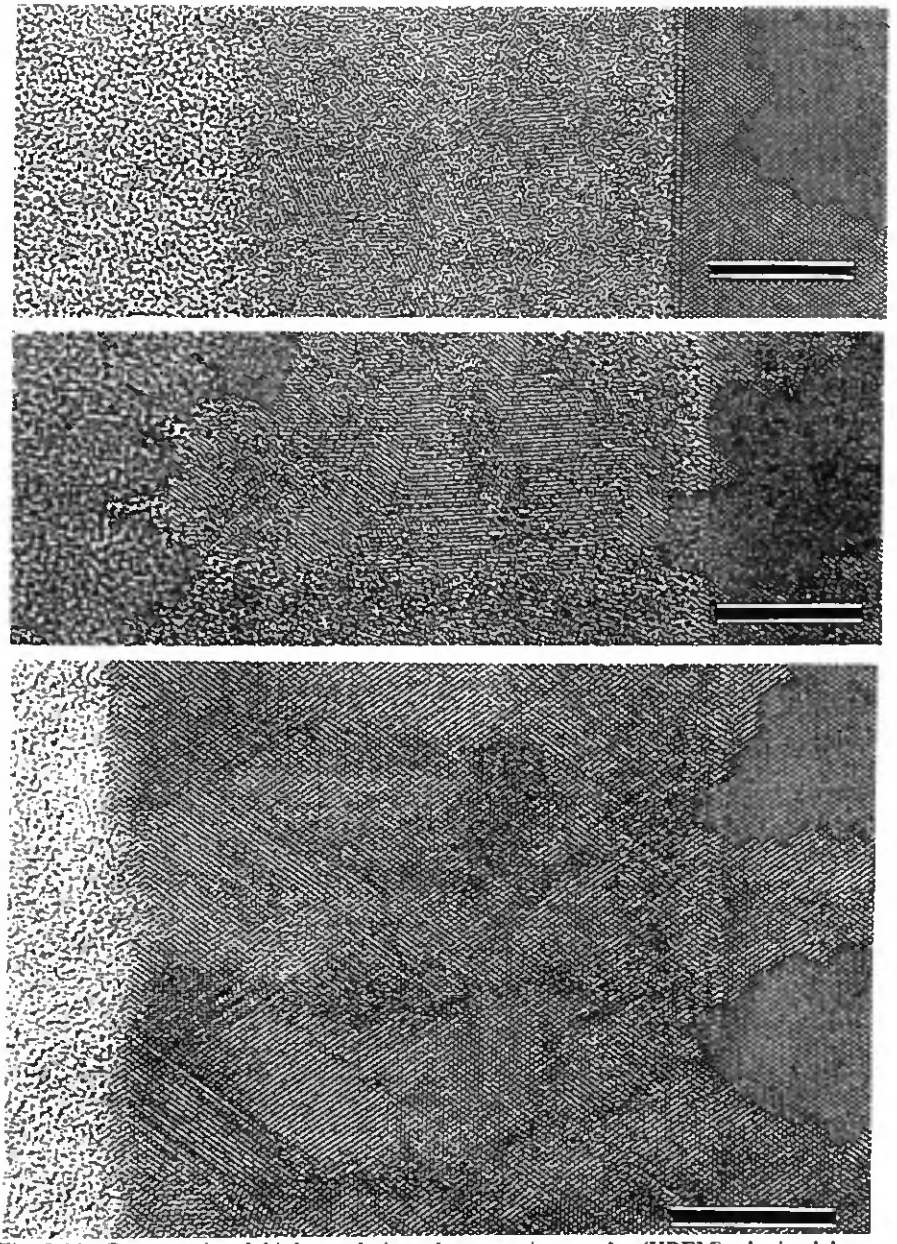

Fig. 2.11: Cross-sectional high resolution electron micrograpbs (HREM) obtained by transmission electron microscopy (TEM) of p-type films deposited onto c-Si. From top to bottom: a) without pre-treatment, b) with plasma pre-treatment, c) with HF-dip pre-treatment. The black line corresponds to 100 Å.

III. Intrinsic μc-Si:H

3. 1. Introduction

For quite a long time, μc-Si:H as prepared by GD - plasma has not been considered to be of use as an active photovoltaic material; it was considered to be difficult to collect the carriers photogenerated in such layers. Research on μc-Si:H layers was limited essentially to the study of doped μc-Si:H layers; these layers are interesting in the formation of p/i and i/n barriers, because of the higher doping efficiency observed in these layers when compared to a-Si:H. It was generally assumed that μc-Si:H is necessarily a defect-rich semiconductor and that therefore such a defect-rich material cannot be used as active layer in a solar cell [46]. The strong n-type character generally observed in as-deposited undoped μc-Si:H was taken as a further fact to corroborate the idea of μc-Si:H basically being a defect-rich semiconductor. Nevertheless, oxygen contamination was already mentioned as an alternative explanation for the n-type character [47]. It was also not clear what gap should be attributed to μc-Si:H. Indeed, in the literature it can not be found that μc-Si:H has a gap of 1.12 eV (like c-Si) as has been shown in a recent publication [48, 49].

A further reason why μc-Si:H was not seriously studied for photovoltaic applications, was the dissuasively long fabrication times that were required for such layers in the case of standard deposition techniques [50-52]. Typical reported deposition rates were below 1 Å/s. This means e.g. that at a rate of 1 Å/s a deposition time of more than 8 h is needed to obtain a typical absorber thickness of 3 μm (!) Luckily, higher deposition rates can be obtained by using newer deposition methods such as the VHF-GD technique. These deposition techniques often not only lead to higher deposition rates, but also often favour crystallisation as is shown in chapter II and IV, and one thus obtains μc-Si:H layers that are different in nature from those obtained with the earlier deposition techniques.

The strong n-type character of as-grown μc-Si:H can also be circumvented: a first way of doing this is to use the so called "microdoping technique", where small amounts of diborane are incorporated into the film; thereby a minimum in the dark conductivity and a maximum in the activation energy can be reached; this demonstrates the feasibility of compensated "midgap" μc-Si:H (where the Fermi level is in the middle of the gap). In the course of such microdoping experiments our group could further demonstrate that the use of "midgap" compensated μc-Si:H as the absorber material in solar cells [53] is one of the important conditions to obtain a high collection of carriers (at least if p-i-n type solar cells are used). Thus, the key to p-i-n type solar cells with μc-Si:H as an absorber material is to

fabricate the latter in the form of a "midgap" material. In fact, p-i-n (or n-i-p) type solar cells which incorporated a μc-Si:H absorbing layer with a too high (slightly p-type) or a too low (slightly n-type) microdoping level showed a significantly reduced carrier collection capability [53]. This is in contrast to the situation observed for crystalline silicon (c-Si) wafer based solar cells, where pn or np junctions are generally used and, where there is no need of "midgap" intrinsic layers. In the case of μc-Si:H solar cells with a p-i-n (or n-i-p) structure the built-in-field (created within the intrinsic layer by the doped layers of opposite polarity) can only be extended over the whole thickness of the intrinsic layer if the latter has a midgap character. Slight (unintentional) doping of the intrinsic layer causes a deformation (reduction) in the internal electric field and consequently a collapse of the carrier collection and thereby a much lower photovoltaic performance is observed.

In the first part of this chapter we will review the "microdoping" technique with the goal of showing that this approach leads to reasonable results: "Microdoping" is obtained by adding diborane in the parts per million (ppm) range into the gas phase during the deposition. Though viable to obtain compensated material, this "microdoping" approach which is unfortunately technologically difficult to handle is certainly not adequate for potential industrial applications, however it indeed "opened the door" to the use of μc-Si:H as a new thin-film semiconductor PV-material. To take full advantage of μc-Si:H, it became therefore highly desirable to find an alternative approach that is simpler to work with.

For that, we had to consider some material properties closer: In the earlier literature it was suggested that both donor-like native defects within the layers and the rather large content of oxygen impurities (10^{19} - 10^{21} atoms/cm^3) could be responsible for the unwanted n-type behaviour [47, 54]. (Thereby one should not exclude the possibility that the μc-Si:H layers deposited by standard 13.56 MHz GD [47, 54], is indeed a defect-rich material witb a much higher defect density than our present VHF-GD layers; this could be in relation with the much higher peak energy of ions observed at 13.56 MHz excitation frequency when compared to the situation prevailing in VHF-GD [55]). Conceptually, by microdoping one can counterbalance both possible effects (donor-like native defects and oxygen impurities) and it was therefore not clear which effect was actually dominating. Nevertheless, it should be noted that the problem of oxygen being a donor-like impurity is a well known effect in c-Si and has been extensively studied in the context of wafer processing, since not only electrical but also mechanical properties are strongly affected and dependent on oxygen contamination. Thus, a short literature review on this effect will be given for the purpose of comparison.

The first important question is, can we reduce the large amount of oxygen detected in as-grown μc-Si:H films? And further, is there a way to distinguish between native defects and electrically active contaminants? As shown for the first time in this thesis, we will demonstrate that oxygen contamination is indeed mainly responsible for the n-type behaviour of our μc-Si:H (as deposited by VHF-GD) and that one can therefore omit microdoping if the

oxygen content is sufficiently reduced in the deposited layers [56]. This approach of controlling the oxygen contamination allowed us not only to successfully replace the earlier "microdoping" technique, but has moreover a strong and beneficial impact on device performance: One thereby obtains intrinsic layers with a low defect density and the control of the whole deposition process is improved. Thus, thicker diodes became feasible and substantial improvements for entirely μc-Si:H solar cells could be achieved.

In wafer-based multicrystalline silicon, where the grain boundaries are only partially (or not at all) passivated, key issues are to obtain "pan-cake" crystallites so as to minimise the grain boundary density along the operating direction of pn - junctions in the initial stage and to subsequently passivate such grain-boundaries by atomic hydrogen. It is remarkable that by such a passivation the electrical properties of these solar cells can be improved, because we are dealing here with cells made of wafers with a typical thickness of about 400 μm. This is only possible because atomic hydrogen, obtained e. g. by a GD-plasma of hydrogen, has a very high mobility within c-Si. An enhanced mobility along grain boundaries is certainly also beneficial. The general observation for such a post-hydrogenation treatment is that it is more effective the poorer the quality of the starting material is [57].

The high grain boundary density as present in μc-Si:H was a priori assumed to favour carrier recombination, as occurs in poly- and multicrystalline silicon. However, deposition of μc-Si:H under GD conditions at low temperatures allows for a very efficient grain boundary passivation by hydrogen during the deposition process itself. Too high temperatures, i.e. temperatures of well over 500 °C (as used in CVD of polycrystalline Si) will not allow the incorporation of enough atomic hydrogen and, furthermore, hydrogen out-diffusion will also occur. From the material point of view progress in solar cell performances was mainly expected by approaching more and more the ideal structural case of having a single crystal (thus the "pan-cake"-approach). Therefore, a material like μc-Si:H, with typical grain sizes of the order of 10 to 1000 Å was not believed to have the potential for ever becoming a photovoltaic material, i.e. a material where photogenerated carriers can be collected before they recombine precisely because of the very high density of grain boundaries. However, it turned out that by using our VHF deposition method at low deposition temperatures, a very efficient grain boundary passivation by atomic hydrogen takes place during the deposition process itself, leading, thus, to very low defect densities. This is evidenced by an estimated defect density of about $5 \cdot 10^{15}$ 1/cm^3 as obtained from CPM - spectra, where one can immediately see that the defect-connected absorption is indeed very low [58, 59].

3.2. The approach of compensation by microdoping

In 1983 it was shown by Spear et al. [60] that as-grown undoped μc-Si:H which has a strong n-type character can be compensated by 20 kV B-implantation followed by a 300°C annealing. This annealing temperature is unusually low for annealing defects created by ion-implantation but it is certainly low enough to avoid hydrogen effusion of the specimen. In fact, very low dark conductivity of below 10^{-8} S/cm could be demonstrated by this technique as shown in fig. 3. 1.

Later, this approach of low-level doping or "microdoping" as we will call it here was followed up by the group of Lucovsky [47, 54, 61-63]. First well rectifying diodes and a relatively strong photovoltaic effect (open circuit voltage of 0.4 V) could be demonstrated by incorporating such compensated μc-Si:H in a p-i-n diode. The deposition technique thereby employed were the so-called "Remote PE-CVD" supplemented by adding small amounts of diborane to the gas phase and, later also, reactive magnetron sputtering where the amount of incorporated boron was controlled by switching between an undoped and a boron-doped target during deposition. Evidence for the inherent stability of μc-Si:H films against light-soaking was also already given. Unfortunately, to the best of our knowledge no ulterior results on incorporating such compensated layers into photovoltaic solar cells have been published.

In our group, the microdoping approach to obtain midgap μc-Si:H was investigated within the framework of the VHF-GD deposition technique [53, 64, 65]. Higher deposition rates and "cleaner" deposition systems may have been responsible for the lower dark conductivities (10^{-3} - 10^{-5} S/cm) obtained for our undoped and uncompensated layers as compared to the undoped specimens reported by Spear et al. (10^{-2} S/cm) (see fig. 3.1.). Further, successful implementation of compensated, i.e. microdoped μc-Si:H into a p-i-n solar cell lead to consistently stable p-i-n solar cell conversion efficiencies of up to 4.6 % as reported by J. Meier et al. [53]. For the first time, such fully microcrystalline solar cells were incorporated into a stacked μc-Si:H / a-Si:H tandem solar cell structure. Thereby full technological compatibility between the deposition technique for μc-Si:H solar cell deposition and a-Si:H solar cell deposition was demonstrated. 9.1 % initial conversion efficiency combined with a very high short circuit current density of 11.5 mA/cm^2 have been reported for this new type of cell [53]. However, due to process instabilities the maximum thickness of the μc-Si:H cell was at the moment (1994) limited to about 1.6 μm.

As can be perceived from fig. 3. 1. the microdoping approach of adding small amounts of diborane is technologically "cumbersome": the process window is narrow and strongly depends on preparation conditions and chamber history; though feasible, this approach is not viable for an industrial process. As can further be seen in the same figure, the dark conductivity of undoped samples decreases as the deposition rate increases. On the other hand

compensation is not achieved at continuously lower microdoping levels as may be expected, indicating, thus, that even if similar deposition conditions are used, different types of μc-Si:H materials may result. Experimenting under such conditions is very time-consuming since for every set of otherwise fixed deposition conditions one has to find again the optimum of diborane microdoping level for compensation. Therefore it is obvious that if we want to reach out for new deposition conditions (e.g. if we want to vary the deposition parameters so as to be able to increase the deposition rate) it would be highly desirable to find another technological approach that is technologically easier to handle than "microdoping".

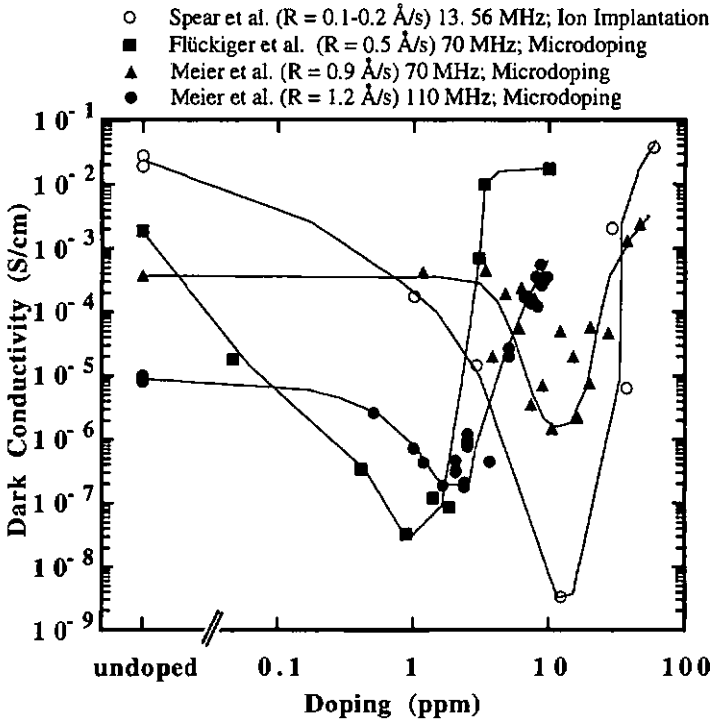

Fig. 3.1. Dark conductivity versus diborane doping level in various low-level doping experiments. The open symbols are data taken from Spear et al. [60] and correspond to ion-implantation experiments performed after deposition of the undoped films. Filled symbols correspond to μc-Si:H deposited by the VHF-GD; compensation is achieved by the so-called "microdoping" approach, i.e. by adding small amounts of diborane to the gas phase during deposition (Data taken from [53, 64, 65]). Different deposition conditions (e.g. RF-frequency, applied VHF - power level) require each time a new adjustment of the compensation point. Note also that for undoped specimens an enhanced deposition rate results in lower dark conductivities.

Furthermore: At this stage of our knowledge it was not yet clear whether the n - type character of μc-Si:H was mainly due to donor - like defects or due to incorporated oxygen impurities that both can be counterbalance by "microdoping".

3. 3. The "intrinsic" approach

3.3.1. *Dark conductivity for intrinsic monocrystalline silicon*

Let us first estimate the order of magnitude of the room temperature dark conductivity in intrinsic monocrystalline silicon so that we have a rough idea for comparison purposes. In an intrinsic semiconductor continuous thermal agitation (thermal emission) exists, which results in a certain number of electrons being able to overcome the forbidden gap. In a fully intrinsic silicon crystal, electrons in the conduction band can only come from formerly occupied valence band levels, thus leaving holes behind them, which results in $n = p = n_i$ and the intrinsic conductivity at 300 K can be calculated for c-Si according to [66], p. 45, as:

$$\sigma_i = q n_i \left(\mu_n + \mu_p\right) \tag{3.1.}$$

thereby we will use some "ideal" values for the electron and hole mobilities (i.e. the highest experimental Hall mobilities measured in single crystals):

- $\mu_n = 1900\ cm^2/Vsec$ and $\mu_p = 495\ cm^2/Vsec$ (bandgap mobilities)

as well as the following parameters

- $n_i = 1.4 * 10^{10}\ cm^{-3}$ (intrinsic carrier density)
- $q = 1.6 * 10^{-19}$ C (elementary charge), all data from [66],

obtaining, thus, for c-Si an intrinsic room temperature conductivity of about

$$\sigma_i = 5 \cdot 10^{-6}\ S/cm. \tag{3.2.}$$

As the intrinsic carrier density n_i can be expressed as (see e.g. [67]) :

$$n_i = \sqrt{N_C N_V}\, e^{Eg/2k_BT} \tag{3.3.}$$

where $N_{C,V}$ are the effective density of states in the conduction and valence band respectively; Eg is the bandgap, k_B Boltzmann's constant ($1.38 \cdot 10^{-23}$ J/K) and T the

absolute temperature, we see that σ_i depends exponentially on the gap Eg, and therefore the latter value has to be known precisely.

The first equation (3.3.1) may be rewritten as:

$$\sigma_d(T) \propto e^{\frac{Eg}{2}/k_B T}, \tag{3.4.}$$

where $\sigma_d(T)$ is the conductivity measured in the dark. Thus, if we plot measured values of ln σ_d versus 1/T we obtain a straight line and can extract the value of the gap. This holds, however, only if other temperature dependencies (Eg, μ) are negligible or cancel out.

3.3.2. Oxygen in crystalline Si

Oxygen together with carbon are the most common unintentional impurities in c-Si [4]. Apart from their introduction through the original feedstock material, oxygen and carbon are incorporated in the melt during crystal growth through the ambient gas and the contact with the crucible; finished wafers reflect in their radial distribution of impurities the specifically pulling characteristics of the crystal that were applied. Oxygen is generally present in Czochralsky-type silicon in relative high concentrations of the order of 10^{18} cm^{-3} [4, 57, 68].

The solubility of oxygen in c-Si, that is the concentration of oxygen that is accepted in solid solution in the host lattice is relatively high. However, precipitation occurs when the oxygen concentration exceeds a threshold value of about $6.4 \cdot 10^{17}$ atoms/cm^3 [4]. The solubility of oxygen in solid silicon decreases with decreasing temperatures. This means that when a crystal contains oxygen at its maximum solubility at high temperatures (e.g. during the Czochralsky pulling process) it becomes supersaturated when it is cooled down. The degree of supersaturation is expressed as the ratio between the capabilities of solubility at the higher and at the lower temperature. Phase equilibrium is reached by the precipitation of impurity atoms that are in excess of the actual solubility. This precipitation occurs in a pbase of different composition and structure. Thereby a strain is created in the crystal due to volume mismatch between the precipitate and the lattice. The consequence is that these precipitates act finally as sites for defect generation in the crystal.

In an as-grown silicon crystal, over 95 % of the oxygen atoms occupy interstitial lattice sites [4]. The remainder polymerises into complexes such as SiO_4. This configuration acts as a donor centre and changes the resistivity of the wafer, as observed also with intentional doping. This donor centre dissolves at annealing temperatures at 700 °C; however this dissociation occurs at the expense of creating other defects. Several temperature ranges are

reported as resulting in specific defects and complexes [69]; furthermore increased solubility of oxygen (as well as of carbon) is reported at higher doping levels; this fact is mentioned here merely to illustrate the complexity of the problem of unintentional incorporation of oxygen.

As an unintentional impurity, oxygen has, apart from the drawbacks mentioned above, the effect of improving the mechanical strength of wafers. This is a highly desired feature since it facilitates wafer handling and avoids wafer warpage. This effect is enhanced by increasing the oxygen concentration up to the solubility level.

In fig. 3.2. (some) measured ionisation energies for oxygen impurity in Si are illustrated [4]. As can be seen, oxygen also introduces deep levels which may act as recombination centres. For our further work, we shall, however, mainly remember that oxygen in silicon acts as a donor- like impurity with a level of Ec-0.16 eV.

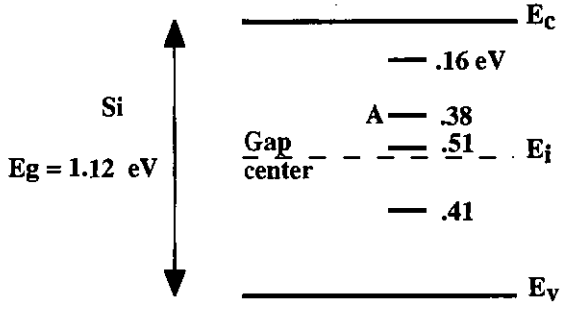

Fig. 3.2. Measured ionisation energies for oxygen impurities in c-Si [4].

3.3.3. Oxygen in μc-Si:H

In earlier publications, it was reported that as-grown μc-Si:H contains quite a lot of oxygen [70]. For μc-Si:H layers deposited in our group the reported concentration of incorporated oxygen is $2 \cdot 10^{19}$ (at/cm^3) as measured by SIMS [20]. This is a high contamination level for undoped layers and, therefore we have carefully analysed possible oxygen contamination sources. Thereby, three different experimental conditions that have an effect on the oxygen content in both a-Si:H and μc-Si:H layers have been identified by U. Kroll et al. [9, 71, 72] :

1. The outgasing rate

Since 1 mbar l/s corresponds to about 60 sccm, a relatively low outgasing rate of about $2 \cdot 10^{-6}$ mbar l/s corresponds already to a flow of impurities (especially of water-vapour from the reactor walls) of about $1.2 \cdot 10^{-4}$ sccm. For a typical silane gas flow of about 5 sccm this means that the outgasing rate alone corresponds to a contamination factor of roughly 20 - 40 ppm (!). Though irrelevant for doped layers, since here the typical gas pbase doping levels used are higher than 1000 ppm (e. g. for p-layers one typically uses 0.5 % diborane in silane), such a level of oxygen contamination in the gas pbase may not be negligible wheo dealing with intrinsic layers. Looking at fig. 3.1 we can get a feeling of the order of magnitudes involved: Microdoping by means of adding small traces of diborane to the gas phase is performed in the ppm level, i.e. at about the same level as oxygen contamination is observed due to outgasing. Owing to a better doping efficiency of boron as compared to the "incorporation efficiency" of oxygen, the situation prevailing when one tries to obtain compensated µc-Si:H is not as "hopeless" as one may deduce from these estimations; however, it is clear that the outgasing rate is indeed an important factor.

2. The feedgas purity

In our laboratory it could be identified that an important source of impurities originates from the feedgas. By using a getter-based metallic-alloy gas purifier (SAES getters) in the gas pipe just before the chamber, this source of contamination could significantly be reduced. According to the specifications on the data sheet of the gas purifier, the quoted outlet impurity levels should be:

O_2:	less than 2 ppb	(parts per billion)
H_2O:	less than 10 ppb.	

Kroll et al. [9, 71, 72] have demonstrated that both a low outgasing rate and the use of the gas-purifier are the necessary conditions to significantly reduce the oxygen content in a-Si:H as well as in µc-Si:H layers.

In fig. 3.3. the oxygen contamination as determined by SIMS measurements performed on µc-Si:H layers are shown. These layers were deposited by applying the gas purifier in most cases; however, they were deposited at different outgasing levels of the deposition reactor. For the purpose of comparison a film deposited without purifier but at a relatively low reactor outgasing rate was also deposited. When applying the gas purifier, we observe that the oxygen contamination in the layers scales with the outgasing rate of the reactor. At relatively high outgasing levels of $6.5 \cdot 10^{-6}$ mbar l /s the gas purifier is of no or little help, impurities from

the chamber walls are sufficient to contaminate the layer with an oxygen concentration higher than $3 \cdot 10^{20}$ l/cm^3. If the µc-Si:H layer is deposited without applying the gas purifier but at a fairly low outgasing rate of below $2 \cdot 10^{-6}$ mbar l/s the oxygen contamination is still about $4 \cdot 10^{19}$ l/cm^3. Only when both a very low outgasing rate prevails and the gas purifier is applied, a successful reduction of oxygen impurities of the layers down to values as low as $2 \cdot 10^{18}$ l/cm^3 can be achieved.

3. The deposition rate

In the case of a-Si:H, it has been shown that the incorporated oxygen content scales to 1/deposition rate [71]. This leads to a model where impurities are incorporated into the layer during growth and thereafter buried by the ongrowing layer. Because VHF-GD has the advantage of an inherently higher deposition rate as compared to standard GD at 13.56 MHz (for both a-Si:H and µc-Si:H) fewer contaminants will be incorporated.

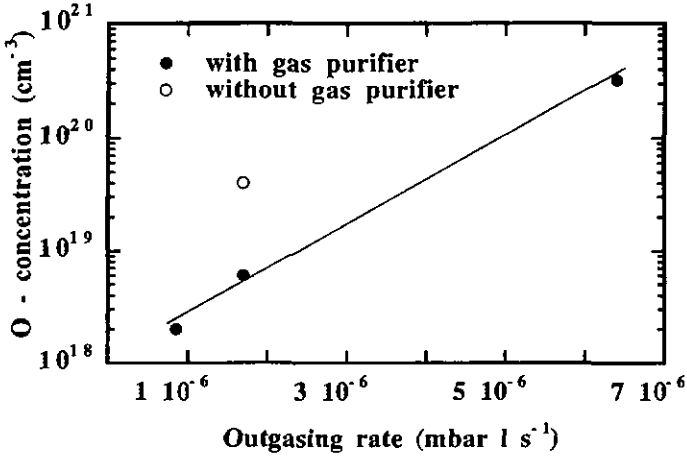

Fig. 3.3. Oxygen concentration in µc-Si:H layers as determined by SIMS measurements in function of the outgasing rate of the deposition reactor. A low outgasing rate and the use of the gas purifier (applied to the source gas lines) are the two conditions that have both to be fulfilled if one wants to obtain films with low oxygen contamination. All these layers are deposited at a dilution level of 2.5% of silane in hydrogen and at a deposition rate of 0.9 Å/s. All data points are taken from Kroll et al. [72].

The important question now is, to know if the reduction of the oxygen content in µc-Si:H layers as elaborated by Kroll et al. (see fig. 3.3.) affects the electrical properties. In order to answer this question, we measured the dark conductivity as a function of temperature

for μc-Si:H layers deposited with different oxygen contamination levels. The absolute oxygen content in the films was assessed by secondary-ion-mass spectroscopy measurements (SIMS).

All the layers were deposited on AF 45 (sodium-free) glass from Schott Co. at a dilution level of 2.5 % silane into a total gas flow of 100 sccm of hydrogen and silane, at an effective substrate temperature of 220 °C, at a power of 6 W (measured at the entrance of the impedance matching box) and at an excitation frequency of 110 MHz. The gas pressure in the chamber was kept at 0.4 mbar. Under these conditions the film growth rate was 1.55 Å/s. The dark conductivity was measured with thermally evaporated Al contacts in a coplanar configuration.

Fig. 3.4. shows, on the left side, the Arrhenius plot of the dark conductivity of three μc-Si:H layers, and on the right side their corresponding values of oxygen content, as measured by SIMS. The layer deposited without the gas purifier shows quite a high room temperature conductivity, in the range 10^{-4} to 10^{-3} S/cm with a very little temperature dependence. This is an indication of a small activation energy and thus of a doped character. The oxygen content of this as-grown "unpurified" layer is about $2.2 \cdot 10^{20}$ atoms/cm^3.

A deposition under the same conditions but with the purifying technique described above leads to a successful reduction of the oxygen content down to $2.5 \cdot 10^{18}$ atoms/cm^3. Electrically the effect is drastic as can be seen in the same figure: by reducing the oxygen content by two orders of magnitude, dark conductivity values at room temperature as low as $2 \cdot 10^{-7}$ S/cm are achievable. These low values are similar to those obtained by the compensation technique based on "microdoping". For comparison, we have plotted in the same fig. 3.3 the conductivity measurement for a compensated microdoped layer (open symbols). This layer was deposited in an equivalent reactor under the same deposition conditions [65]. The activation energy of this compensated microdoped layer is equal to about the half of the optical gap of μc–Si:H (by modelling the true absorption of μc-Si:H, it has recently been shown that the gap is equal to that of c-Si, i.e. 1.12 eV [48, 49]).

To demonstrate further the effect of the oxygen impurity we deliberately contaminated a μc-Si:H layer during the deposition process. Through a needle valve we simulated an air leak into the reactor. Just before causing the air leak, the outgasing rate was $1.1 \cdot 10^{-6}$ mbar l/s and with the controlled leak it then rose up to $1 \cdot 10^{-5}$ mbar l/s. The results are given in fig. 3.4: one sees once again that the resulting oxygen content ($4 \cdot 10^{19}$ atoms/cm^3) correlates with the room temperature value of the dark conductivity. This further experiment evidently demonstrates that the gas purifier is of no or little help if the outgasing rate of the reactor is not low enough.

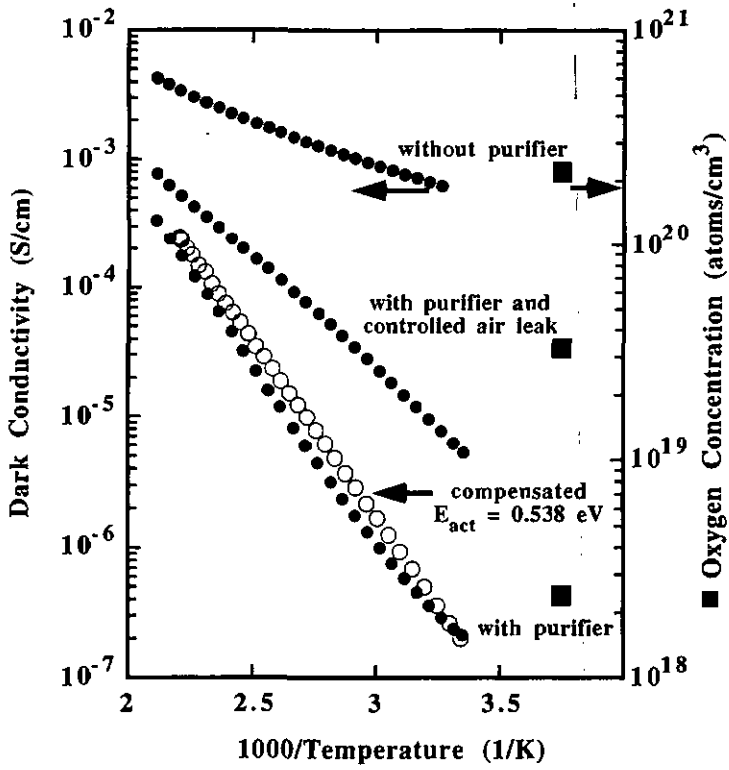

Fig. 3.4. On the left (dots): Arrhenius plots of the dark conductivity (measured in a coplanar configuration) for three μc-Si:H films deposited by VHF-GD with varying oxygen levels, obtained by the use of different purifier/outgasing cooditions. On tbe rigbt (squares): corresponding values of oxygen content (measured by SIMS). For purposes of comparison, data of a compensated "microdoped" at 3 ppm of diborane layer (open circles) deposited in an equivalent reactor under the same deposition conditions, but without a feedgas purifier, is added [65].

3. 4. Impact of the purifier technique on solar cells

The most challenging question with respect to the purifier approacb is however, how will such purified μc-Si:H layers perform in the actual device? Will they perform better than layers obtained with the earlier "microdoping" approach or will they allow only for a mediocre performance in the finished solar cell due e.g. to diffusion of dopants from the contact layers into the intrinsic layer? It was therefore mandatory to implement such intrinsic

μc-Si:H layers grown under the same conditions into fully μc-Si:H p-i-n diodes and characterise their photovoltaic performance.

The cells were grown on SnO_2-coated glass (Asahi type U, with textured surface). Back contacts for the cells were made in-house and consist of highly textured ZnO [73, 74] and Ag. The n- and p-type doped layers used in the p-i-n cell were the same as those described in previous work [18, 20], where a full optimisation of such doped layers was carried out.

Fig. 3.5. shows the spectral response (SR) of entirely p-i-n μc-Si:H solar cells with the i-layers (thickness 2.8 μm) prepared under exactly the same conditions as for the layers studied above (in section 3.3), one with and one without using the feedgas purifier. In previous microdoping studies [53] where one had incorporated midgap μc-Si:H into p-i-n solar cells it had already been shown that the exact properties (i.e. the Fermi level position) of the i-layer have indeed a strong influence on the performance and particularly on the SR of the μc-Si:H solar cell device [53]. It has been shown, that only a small offset in the intrinsic layer from the compensation level, i.e. only a small offset of the Fermi level from midgap is sufficient to strongly reduce the carrier collection in the resulting p-i-n solar cell. As can be seen in fig. 3.5, reduction in the oxygen content of the intrinsic layer obtained by applying the gas purifier is remarkable and leads indeed to a substantial enhancement of the SR. The spectral response of the cell deposited without purifier is mainly reduced in the long wavelength region. This indicates that the i-layer is contaminated and has a n-type character: The electrical field is mainly present at the front of the cell, i.e. we are dealing here with a p^+nn^+ structure and not with a p-i-n structure.

In comparison with the delicate compensation technique where the device thickness had to be limited to 1.6 μm if one wanted to obtain solar cells with reasonable conversion efficiency (up to 4.6 %), now even thicker devices (here: 2.8 μm) which still allow to separate and collect the photogenerated carriers could be successfully prepared. This may be due both to the reduction in contamination level as well as to a better control of the deposition process. In fig. 3.5. it can be seen that applying the gas purifier results in a substantial increase of the spectral response (gain of photocurrent of about 2), leading to a cell conversion efficiency of 5.3 %.

Note that the device described here was the first μc-Si:H solar cell which was prepared with a reduced oxygen contamination thanks to the purifier approach. In the meantime conversion efficiencies have progressed by better process optimisation (e.g. interfaces) and now the usual device thickness in our laboratory is around 3.5 μm.

Degradation experiments on this μc-Si:H solar cell support our earlier claim that μc-Si:H can be considered as a photovoltaically stable material: Exposure to a high-pressure sodium lamp at about 8 suns intensity, for a time period of 264 h and at a temperature of 50 °C did not show any light-induced degradation effect, as represented in fig. 3.6.

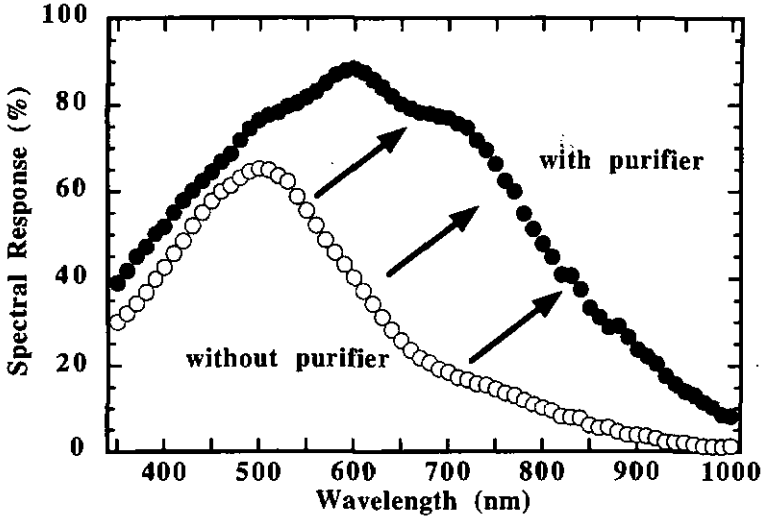

Fig. 3.5. Comparison of the spectral response (at zero bias voltage) of two entirely μc-Si:H cells: One produced with and one without a feedgas purifier. The thickness of both cells is 2.8 μm.

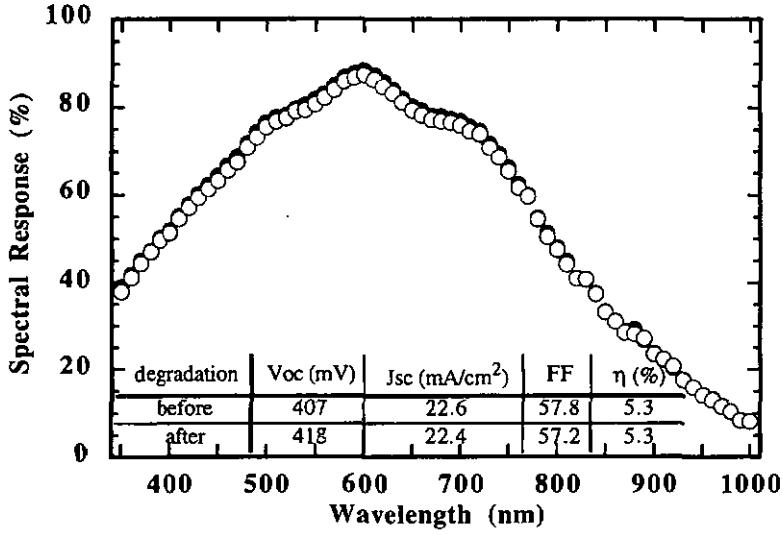

Fig. 3.6. Spectral response of a 2.8 μm thick fully μc-Si:H solar cell produced with the feedgas purifier before and after light soaking (high pressure sodium lamp with an intensity equivalent to 8 sun during 264 h at 50 °C).

3. 5. Conclusions

In conclusion, we have shown that a reduction in oxygen impurities acting as unwanted donor states leads to a strongly improved "photovoltaic quality" of the active thin-film silicon material, i.e. intrinsic μc-Si:H layer, as used in the p-i-n cell. One can speculate that such μc-Si:H films with low oxygen content may also improve the performance of microcrystalline silicon thin-film transistors. The reduction of oxygen contamination can be achieved by simultaneously controlling the outgasing rate of the reactor and applying a feedgas purifier. An increased deposition rate (as favoured by the VHF-GD) also leads to a lower incorporation of impurities when compared with low-growth rate deposition processes. With the help of this purifier technique it is easier to search for new deposition conditions (e.g. for a further increase in the deposition rate) since there is no more need for readjusting the compensation level, as was previously the case with the microdoping approach.

The purifier technique results in a substantially enhanced device performance i.e. in higher solar cell efficiencies than the earlier microdoping approach (5.3 % for the first cell produced with the purifier approach instead of 4.6 % for the best cell produced with the microdoping approach). In the same year after introducing this purifier approach, a single-junction p-i-n cell with 7.7 % conversion efficiency could be realised with this technique; this cell had a thickness of 3.6 μm [65]. We have thus successfully replaced the earlier microdoping approach by the purifier approach. Within our VHF-GD process, conversion cell efficiencies have now almost doubled since introducing the purifier approach: In the latest publications, 8.5 % single junction and stable 12 % micromorph conversion efficiency have been reported [75, 76].

IV. INCREASING THE DEPOSITION RATE OF μc-Si:H

4.1. Introduction

4.1.1 Motivation

Up to now doped μc-Si:H layers have mainly been used as window layers for solar cells or as contact layers in TFT's at a very low thickness of only 100 - 200 Å [14]. For such applications, typical deposition rates of about 1 Å/s were not at all a problem. However, in our case, as we want to use undoped μc-Si:H as an absorber material for the sunlight the situation is different: in order to absorb enough sunlight, the required μc-Si:H layer thickness is about 3.5 μm [65, 75] and consequently the low deposition rate of μc-Si:H becomes a major concern.

This fact is illustrated in fig. 4.1. where the time required to obtain a layer thickness of 3.5 μm is given for different deposition rates. Note that these are net deposition times. One can see that the deposition of the active intrinsic layer lasts about 10 h if a usual deposition rate of 1 Å/s is employed. A much more reasonable deposition time (for laboratory work) would be about 2 h (allowing 1 - 2 layers or cells per day) which could be achieved with a deposition rate of about 5 Å/s. However, a further increase to at least 10 Å/s with a significant decrease of the reactor occupation time would be necessary to render the process attractive for an industrial implementation.

Currently, investigations to reduce the necessary absorbing layer thickness to about 1 μm by using light trapping schemes are also under way. However, even there, higher deposition rates than the usual 1-2Å/s are necessary to obtain a sufficient throughput. In the middle of interest are reduced absorber layer thickness (≈ 1 μm) and simultaneously high deposition rates (> 10 Å/s) as the global target for PV-devices is cost reduction. In this context, the VHF-GD technique has already proven its effectiveness in achieving a high deposition rate of device grade a-Si:H [5, 8, 9].

High deposition rates and μc-Si:H growth conditions are a priori not necessarily contradictory. In fact, it has been shown using hot-wire CVD, that very high deposition rates over 40 Å/s for thin film silicon (μc-Si:H / poly-Si) are feasible [77, 78]. However, such fast hot-wire CVD μc-Si:H material is up to now difficult to be incorporated into solar cells. Very first results on cells containing such thin film silicon layers showed 3 % conversion efficiency for the hot wire technique at a deposition rate of 5 Å/s [79].

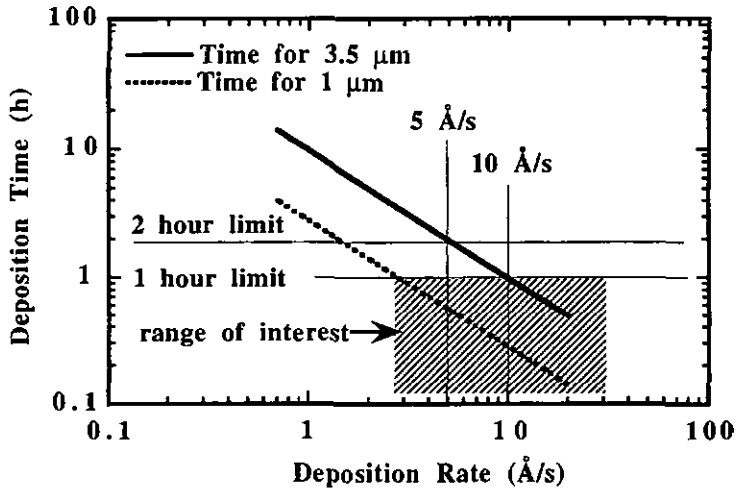

Fig. 4.1. Deposition time required for an intrinsic µc-Si:H layer of 3.5 µm (today's thickness of a µc-Si:H solar cell) and 1 µm thickness for different deposition rates.

The results shown in chapter 2 about high quality p-type µc-Si:H deposited at higher rf-frequency and also higher deposition rates motivated us to further investigate in this direction since the found larger parameter space indicates that there is still margin for improving the deposition rate.

Further, the purifier approach available now allows a direct implementation of the undoped layers into solar cells.

4.1.2 Experimental approach

The growth of µc-Si:H is usually achieved at high dilution levels. This is one of the reasons why generally only low deposition rates are obtained. Owing to hydrogen-dilution of silane, low flows of silane may not allow to create a high density of precursors. The best illustration for this argument is given by the hot-wire CVD, where the pyrolitic decomposition of the source gas (also hydrogen-diluted silane) results in a very high radical creation and thus indeed gives rise to very high deposition rates. E.g. it has been shown, that a deposition rate of 37.1 Å/s [77] can be achieved with the hot-wire CVD technique with a flow of silane of only 2 sccm. To the best of our knowledge, in the case of PECVD, such a low flow of silane has never resulted in a deposition rate exceeding about 2 Å/s! Thus, the low silane flow due to dilution is indeed a major reason for low deposition rates, but, in addition, the little available

silane is poorly decomposed into precursors which further contributes to slow growth. Furthermore, the slowly growing layer is partially etched by the hydrogen rich plasma and it cannot be avoided that some of the VHF-power is consumed for the H_2 dissociation.

We therefore have basically two possibilities which may allow us to speed up μc-Si:H growth: first, increasing the silane concentration of the source gas (that means less dilution) and second, increase of the decomposition rate of silane into precursors (e.g. by increasing the power fed into the plasma). As will be shown in the following sections, we successfully followed up both directions.

In a first series we will show that an increase of the silane concentration of the source gas (less diluted) results indeed in an increased deposition rate. However, this approach is limited since we obtain a-Si:H when the dilution is not high enough. Furthermore, depending on the deposition conditions (e.g. excitation frequency, total gas flow, etc.), the dilution level where the morphological phase transition occurs changes and this approach is limited to deposition rates below about 3 Å/s.

Then we fix the dilution level and vary the applied VHF-power. Thereby we found, that deposition conditions at higher silane concentration (less dilution) can be maintained in the μc-Si:H growth regime, provided that the applied VHF-power level is high enough. By this approach high quality μc-Si:H materials with deposition rates in excess of 10 Å/s could be achieved. First incorporation of this material into single-junction n-i-p devices showed e.g. 5.2 % conversion efficiency at a deposition rate of 10.9 Å/s. To the best of our knowledge, this is the highest deposition rate reported to the date of writing of this report for a μc-Si:H absorber material in a solar cell.

Although we were able to demonstrate that the VHF-GD deposition technique has indeed the unexploited potential for high depositions rates of device grade μc-Si:H, the quest for the most optimal deposition condition is a complex and very time consuming work. In fact, the possible parameter space given by the process parameters such as excitation frequency, dilution level, total gas flow, temperature, VHF-power, substrate temperature, etc. is enormous. Furthermore, the process parameters usually do not change in a linearly dependent way. A systematic elaboration of the whole parameter matrix by depositing and analysing a large number of layers is, thus, a rather questionable approach. It would be more adequate and efficient to dispose of a plasma monitoring tool that allows to predict - in a certain extent - the potential deposition rate as well as the morphology of the ongrowing layer. To this end we used optical emission spectroscopy (OES) for plasma monitoring, since once calibrated for one particular set-up, it may elucidate in which parameter range μc-Si:H or a-Si:H growth occurs. Such OES measurements were done for two series, where process parameters were scanned that were known beforehand to show a morphological transition from a-Si:H to μc-Si:H growth.

4.1.3. Layers characterisation techniques

The individual μc-Si:H layers were basically characterised by X-ray and IR-absorption to determine their microstructure.

We checked the crystallinity of the materials by performing X-ray diffraction measurements on layers deposited on glass. We will call our material μc-Si:H silicon as soon as diffraction peaks are observable in our set-up. By comparing the intensity distribution of diffraction peaks with that of randomly oriented silicon powder sample, we can also determine the texture, that is whether a preferential orientation of the crystallites with respect to the sample normal plane exists. To get insight in the bonding structure and bonding environment of hydrogen, we performed IR-absorption measurements. With this method it is also possible to determine the total bounded hydrogen content in the layers.

Further, the optical absorption was measured. In earlier studies it bas been shown, that μc-Si:H can have an enhanced apparent absorption in the visible and near IR light compared to crystalline silicon [58]. This fact is very important for solar cell fabrication, since the overall enhancement of the absorption coefficient allows one to make considerably thinner cells which still absorb the same quantity of light.

On the other hand, the measurement and interpretation of electrical properties of μc-Si:H is not straightforward as the structure of μc-Si:H is heterogeneous (amorphous and crystalline phase, anisotropy). Furthermore, the characterisation techniques known from a-Si:H cannot be applied directly to μc-Si:H and are still under investigation [59, 80-84].

Also, μc-Si:H layers often suffer from strong postoxidation [85]. As a coosequence, the electrical properties (i.e. σ_d) change with time on a month time scale. This fact renders the electrical characterisation of μc-Si:H layers even more difficult and questionable at this level.

On the other hand, in a recent experiment we have shown [75] that although the dark conductivity in a "state of the art" μc-Si:H layer increased by 3 orders of magnitude due to postoxidation, the conversion efficiency of the cell incorporating this same layer remained constant. This result proves that postoxidation affects μc-Si:H layers, but oot μc-Si:H based solar cells as can clearly be seen in fig. 4.2. The cell design seems to protect the incorporated intrinsic layer from postoxidation; we assume that this due to the doped contact layer. In fact, the cells were exposed to air for more than 1 year before metallisation and did not show any change at all w.r.t. any cell parameters, notably the red spectral response. An indifussion of oxygen from the back side would have affected mainly the light that is absorbed in the back, that is the red spectral response.

These arc the reasons why we will not discuss the electrical properties of individual layers destined for solar cell applications. However, this issue is followed up and addressed in detail elsewhere [86]. In this work we made the choice to incorporate our various layers

directly into solar cells and assess the device characteristics under a solar light simulator together with spectral response measurement.

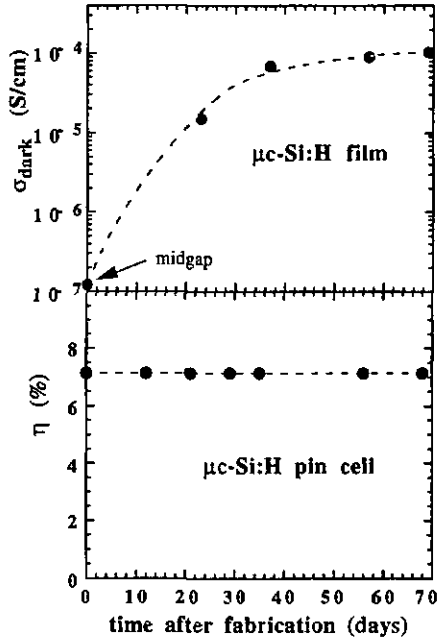

Fig. 4.2. Whereas the dark conductivity of a μc-Si:H layer increases in time due to postoxidation, a stable behaviour of the conversion efficiency of a solar cell incorporating this same layer is observed [75].

X-ray diffraction spectra

All the X-ray measurements presented in this thesis were done at the Physics Institute of the University of Konstanz by Dr. J. Köhler and Dr. U. Mallang. They were done using a commercial Siemens D501 X-ray powder diffractometer by performing θ - 2θ scans. Under these experimental conditions, only those planes parallel to the sample surface and satisfying the Bragg condition will contribute to constructive interferences in the direction of reflection, i.e. towards the X-ray counter. An accelerating voltage of 40 keV at 30 mA is used to produce Cu-K_α radiation having a wavelength of 1.5406 Å. Specimens having a size of about 4 cm^2 are fixed on the sample holder, which is rotated around himself during measurements. The diffracted rays are recorded for 2θ angles ranging from 10 - 80°.

As soon as crystalline diffraction peaks are appearing the crystalline fraction is higher than 40 % for our samples as shown by deconvolution of Raman-spectra [87].

IR-absorption

The IR-absorption measurements between 4000 and 400 cm^{-1} wavenumbers were performed with a Perkin-Elmer Fourier IR (FTIR) spectrometer 1720 X on films deposited on <100> Si wafers. From the IR transmission spectra referenced to a plain Si wafer, the absorption coefficient was calculated according to the procedure described in literature [88-91]. Special care was taken to ensure that the substrate and the reference wafer were from an identical batch to match them perfectly and avoid, thus, a contribution from the substrate c-Si phonon at 615 cm^{-1}. The bounded hydrogen content C_H was obtained by numerical integration of the Si-H rocking-wagging mode at 640 cm^{-1}. The complete procedure can be expressed by the following equations:

$$C_H(at.\%) = \frac{A_W}{N_{Si}} \int_{\nu_{r/w}} \frac{\alpha(\nu)}{\nu} d\nu \approx \frac{A_W}{N_{Si}} \sum_{\nu_{r/w}} \frac{\alpha(\nu)}{\nu} \Delta\nu \qquad (4.1.)$$

where $\alpha(\nu)$ is the absorption coefficient of the film at the wavenumber ν, $\nu_{r/w}$ stands for the rocking-wagging bands around 640 cm^{-1}, $A_W = 1.6 \cdot 10^{19}$ cm^{-2} is the proportionality constant, and $N_{Si} = 5 \cdot 10^{22}$ cm^{-3} is the atomic density of pure silicon. In a recent publication it has been shown that the A_W proportionality constant is the same for a-Si:H and μc-Si:H [91]. The accuracy of the results are about ±15 % of the hydrogen content.

Typical fingerprint patterns at 640, 840, 880, 2000 and 2090 cm^{-1} are associated to H bonding structure in a-Si:H [89, 92]. Simultaneously with the apparition of Si diffraction peaks in the x-ray spectra, new and narrower peaks around 626, 900 and 2101 cm^{-1} arise and progressively replace those of a-Si:H. The latter observation is a clear indication for changes in the hydrogen bonding nature and in the bonding environment. By comparison with the results presented elsewhere [92-95] all these vibration modes as observed for μc-Si:H (i.e. the rocking-wagging, bending and particularly the different stretching modes around 2100 cm^{-1}) can be assigned to mono and/or dihydride bonds on (100) and (111) surfaces of silicon crystallites.

Optical absorption

The typical absorption spectra of different silicon-based materials are represented for comparison in fig. 4.3. The absorption spectra of c-Si [96] shows a parabolic shape related to the indirect nature of the fundamental optical gap at 1.12 eV. The multicrystalline material (p-type wafer with grain sizes ~ 5 mm) basically has the same absorption behaviour as c-Si,

but a detrimental amount of defects appear in the gap due to unpassivated grain boundaries. Contrary to this, the optical gap of a-Si:H is enlarged to around 1.7 eV (Tauc gap) due to the disorder in this material. Its absorption in the region of visible light is strongly enhanced compared to the other materials as the k-selection rule (contribution of a phonon to the absorption process) is relaxed.

The shape of the absorption spectra of a typical high-quality μc-Si:H layer deposited by VHF-GD, in its turn, follows the shape of c-Si over a wide range of energy, but is shifted to lower energies and higher absorption values. Both, the enhancement and the shift of the absorption edge are important advantages for the application of μc-Si:H material in solar cells. In fact, the shift of the absorption edge makes it possible to absorb infrared light of even lower energies, and, furthermore, the overall enhancement of the absorption coefficient allows one to make considerably thinner cells which still absorb the same quantity of light.

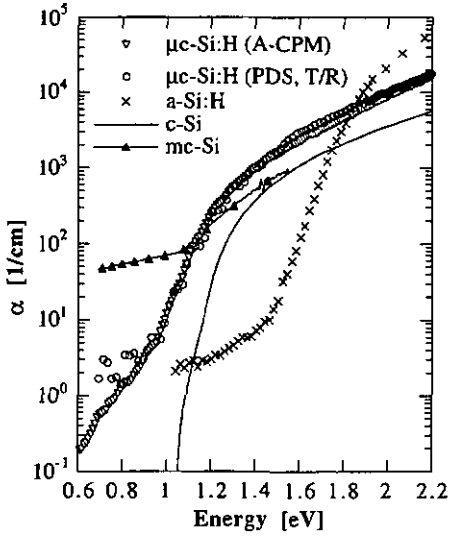

Fig. 4.3. Absorption coefficient of VHF-GD μc-Si:H compared to c-Si [96], a-Si:H and a p-type poly-silicon wafer. The absorption of μc-Si:H has almost the same shape as c-Si, but is shifted to higher values and the apparent bandgap curve is shifted to lower energies (red shift).

The reasons for this absorption behaviour can be manifold as discussed in detail in [58]. However, it has been recently shown [49] that for our μc-Si:H deposited by the VHF-GD the prevailing mechanism responsible for the enhanced optical absorption (compared to c-Si) is surface and volume scattering due to the rough surface and the heterogeneity of μc-Si:H. We

will call this enhanced absorption "**apparent optical absorption**", this is the absorption that is actually relevant for our solar cells.

The defect-connected absorption in device grade μc-Si:H produced by the VHF-GD (see fig. 4.3.) can be very low ($\alpha \approx 1\ cm^{-1}$ at 0.8 eV) and suggests an efficient passivation of the grain boundary defects by hydrogen.

The methods used for the optical absorption measurements are the constant photocurrent method (CPM) and photothermal deflection spectroscopy (PDS) calibrated with T/R measurements. CPM-spectra shown in this work were all performed in close collaboration with the group of Dr. M. Vanecek at the Physical Institute of the Academy of Sciences of the Czech Republic in Prague.

Characterisation of Solar Cells

Solar cells have been measured under a two-source solar simulator (Wacom WXS-140S-10) to extract from the current-tension characteristics the open circuit voltage (V_{OC}) and the fill factor (FF). To get a precise measurement of the short circuit current density (j_{SC}), the spectral response of the solar cells was evaluated and then convoluted with the standard solar spectrum (spectral distribution corresponding to AM 1.5 and a fixed irradiance of 100 mW/cm^2). This procedure allows a reliable calculation of the solar cell conversion efficiency.

4.1.4. Solar Cell Structure

Conceptually, cells deposited in the p-i-n sequence are limited to transparent substrates like glass or some (rare!) highly transparent and temperature resistant polymers, as the light always enters the cell through the substrate in this configuration. To be able to use a wider choice of substrates, including opaque metal sheets with capability for a roll-to-roll deposition process, the inverse n-i-p deposition order has to be applied. In this case, the light enters the cell from the "top" side, i.e. the side opposite to the substrate.

Furthermore, the n-i-p structure shows an additional advantage. The front p-layer of a solar cell is manufactured as thin as possible, since highly doped layers are photovoltaically inactive (dead layers). In fact, this p-layer is empirically adjusted to be just thick enough to build up the field within the cell. Technologically a careful optimisation of this layer together with the successive intrinsic layer and their interfaces is necessary; this means that for a given intrinsic layer the corresponding optimum window layer has to be found. Further, a partial etching of underlying layers in the case of depositing an i-layer is known. Thus, this situation would have been difficult to control and comparison for a wide scan of i-layers implementing into devices delicate.

Therefore, we used for our study only n-i-p structures as shown in fig. 4.4. The n-i-p cells were deposited on SnO_2 coated glass from Asahi company (type U).

A white sheet of paper was simply used as a back reflector, whilst doing current-tension (I-V) and spectral response characterisations. This "test" configuration certainly does not lead to devices with the highest efficiencies, but it does allow for a fast and realistic probe of the layer quality. Furthermore, a transfer on opaque substrates, such as aluminium, stainless steel, etc. is relatively straightforward as we demonstrated in [97, 98].

The cells were terminated by an ITO contact sputtered through a mask of 3 mm diameter. To minimise the lateral collection of the cells, the cells were then mechanically scratched as close as possible to the ITO contact.

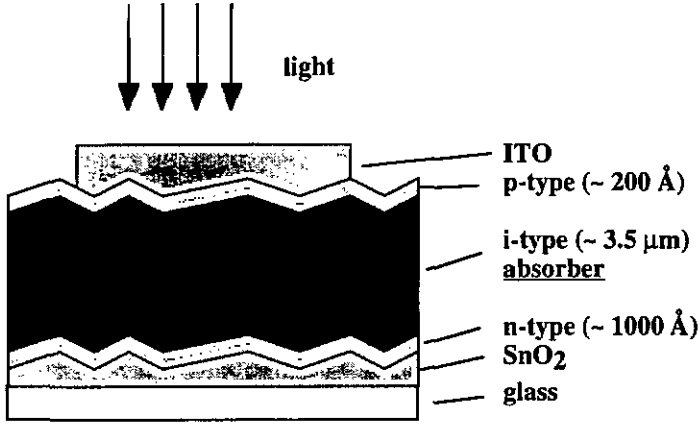

Fig. 4.5. n-i-p structure used for the µc-Si:H solar cells.

4. 2. Dilution controlled morphology

The first straight approach to increase the deposition rate is to provide more fresh silane gas, that is to use a lower dilution. To this end, in a series of samples we systematically increased the silane gas flow ratio from 1.25 % up to 7.5 %, keeping all the other deposition parameters constant (excitation frequency of 110 MHz, low VHF-power input of 6 W, process pressure of 0.4 mbar, effective substrate temperature of 230±10 °C with a total gas flow of 100 sccm). The resulting deposition rate is plotted in fig. 4.5. As expected, a significant enhancement of the deposition rate with increasing silane concentration is observed. However, it is known that μc-Si:H growth usually requires a high dilution of silane with hydrogen and one may therefore expect that the variation of the silane concentration by a factor of 6 will also lead to significant structural changes in the deposited material.

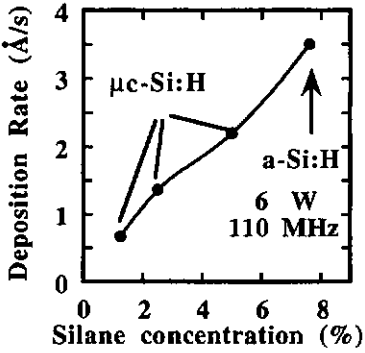

Fig. 4.5. Deposition Rate in function of the silane gas phase ratio.

We therefore examined all the layers of this series by X-ray and by IR-absorption measurements. Both measurements clearly show that the layer deposited with a silane gas phase ratio of 7.5 % is amorphous as no X-ray diffraction peaks are observed (see fig. 4.6.) and only the hydrogen bonding configuration typical for a-Si:H (640, 840, 880, 2000 and 2090 cm^{-1}) is visible in the IR absorption spectra (fig. 4.8.). However, all the other layers produced with lower silane concentrations exhibit X-ray peaks, fingerprints of a crystalline phase in the material. Furthermore, whereas in a randomly oriented crystalline silicon powder sample the intensity of the (220) peak is about 55 % of the (111) peak, in all our μc-Si:H samples the (220) peak clearly prevails, indicating, thus, a preferential growth along the [110] direction. As can be seen in fig. 4.7, the texture is decreased by increasing the dilution. This is

evidenced by the ratio of the (111) and (220) peaks which decreases towards the ratio found in silicon powder diffraction pattern.

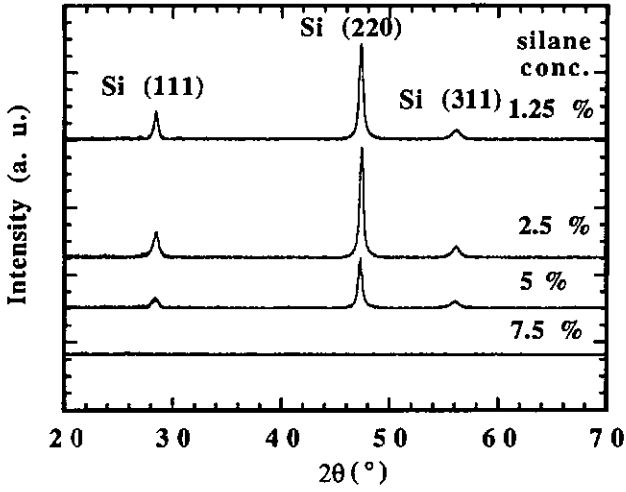

Fig. 4.6. X-Ray diffraction spectra of the dilution series. They reveal a preferential growth along the [110] axis. The layer at a silane concentration level of 7.5 % is amorphous: it shows no crystalline diffraction peak. In fact, because of the evaluation procedure, there is no signal associated to a-Si:H either.

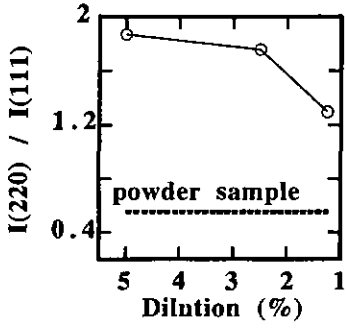

Fig. 4.7. Texture as defined as the intensity ratio of I(220) / I(111). All samples show a clear preferential growth along the [110] axis when compared to the silicon powder sample, where the intensity ratio of I(220) / I(111) is 55 %. Lower silane concentrations (higher dilution) hampers the preferential growth.

Fig. 4.8. shows the IR-absorption spectra. One can clearly see a continuous change of the absorption peaks. The sample prepared at a dilution of 7.5 % retains the fingerprint patterns at 640, 840, 880, 2000 and 2090 cm^{-1} pertaining to a H bonding structure

characteristic of a-Si:H layers. For silane concentrations lower than 7.5 % narrower peaks around 626, 900 and 2101 cm^{-1} arise. Hence IR measurements are as sensitive as X-ray measurements to detect the presence of crystalline phase in our films: the observation of the vibration mode around 2100 cm^{-1} can be taken as the indication of the crystalline phase.

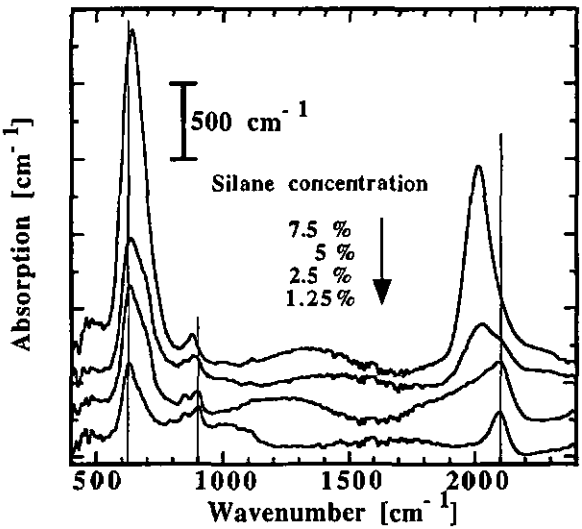

Fig. 4.8. IR - absorption spectra of layers prepared at different silane gas flow ratios as indicated in the figure. The highlighted vibration modes can be assigned to mono/or dihydride bonds on (100) and (111) surfaces of silicon crystallites. The peak at 2100 cm^{-1} occurs simultaneously with the diffraction peaks io the θ-2θ X-ray measurement.

The apparent optical absorption of the different layers given in fig. 4.9. are in quite good agreement with the material structure (see fig. 4.6.). Again, one can see the transition from an amorphous like spectra to a crystalline like spectra [99]. For the μc-Si:H materials, the measured apparent optical absorption steadily increases with dilution due to a transition from a mixed phase material (5 % sample) to a μc-Si:H material with a high crystalline volume fractioo (2.5 and 1.25 %). However, as for the 5 % dilution mixed phase material one of the basic conditions for CPM is not fulfilled [59] and furthermore scattering related enhancement of the optical absorption is observed, an ulterior interpretation at this level is not possible. Unfortunately, the only layer that exhibits the desired enhanced optical absorption is the one deposited with 1.25 % at the lowest deposition rate of only 0.55 Å/s. In addition this same layer shows also the highest defect connected absorption.

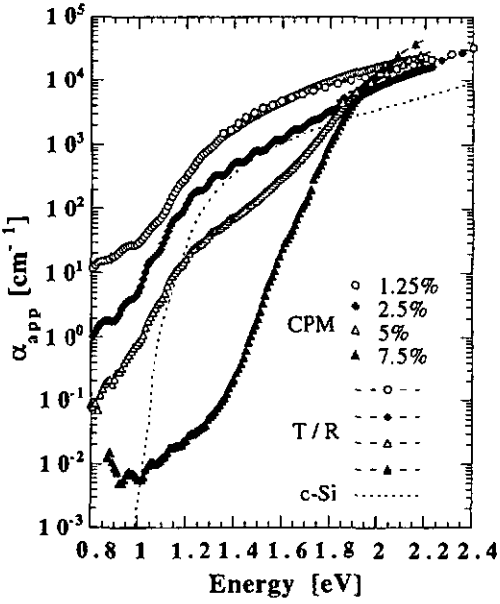

Fig. 4.9. CPM shows that by increasing the silane partial pressure the optical properties change substantially. With reducing the silane partial pressure the measured apparent optical absorption is steadily enhanced [99].

As a conclusion, although reducing the dilution is favourable for enhancing the deposition rate, the optical and structural properties of the obtained materials do not fulfil our requirements. Therefore, this approach will not be used further.

4. 3. VHF-Power Series of μc-Si:H material

4.3.1 Lower ion impact energy due to higher frequencies

Applying higher plasma power levels to increase the deposition rate of μc-Si:H has usually been avoided in the past, since it was argued, that too high power levels may induce too many defects on the ongrowing layer due to ion bombardment. The ion bombardment is due to positive ions impinging on the growing layer. These positive ions gain their impact energy crossing the sheath potential: as soon as they get close to the edge of the sheath, they experience an accelerating voltage towards the substrate.

The sheath potential, in its turn, is estimatively accessible by measuring the peak to peak voltage (Vpp) on tbe powered VHF-electrode (in our reactor configuration with symmetrical electrodes and grounded substrate electrode the self bias is negligible and does not contribute to the sheath potential). By using the capacitance sheath approximation it has been shown, that the time averaged sheath potential equals Vpp/4 resulting in a maximum ion energy at the substrate surface of qVpp/4 [100].

By increasing the excitation frequency, the sheath thickness is reduced [9]. This leads to a reduced sheath potential and thus to a lower ion impact energy. In fact, it has been shown, that an increase of the rf-excitation frequency from the standard 13.56 MHz to the VHF frequency of 70 MHz results (for a fixed effective plasma power of Peff = 5 W) in always lower Vpp - values and thus to a lower ion impact energy [6]. This result explains why under VHF-conditions (70 MHz), it was possible to enhance deposition rates of a-Si:H while maintaining a defect density comparable with that of standard material deposited at en excitation frequency of 13.56 MHz.

This important result motivated us to measure in our own deposition reactor the Vpp - values for a set of frequencies and plasma-power values, also because slight changes on the reactors electrodes had been made. Vpp measurements were performed on the powered electrode with a low capacitive passive probe. First, Vpp values outside of the vacuum vessel were measured (as close as possible to the powered electrode) to calibrate thereby Vpp values as measured directly on the electrode-plate. Then, we measured for 70, 100 and 130 MHz the injected VHF-power (by adjusting the impedance matching capacitances in order to minimise the reflected power) with and without plasma and the corresponding Vpp-values. For a fixed Vpp - level, the (effective) plasma power is equal to the total applied power (with plasma) minus the vacuum power (lost in the network). This is shown in Fig 4.10a. for 70, 100 and 130 MHz. From this graphs we can thus also extract for the effective plasma power the corresponding Vpp value. As a plasma we used conditions known to result in μc-Si:H growth,

i.e. a hydrogen-diluted silane plasma (3 % of silane in hydrogen and 0.4 mbar process pressure).

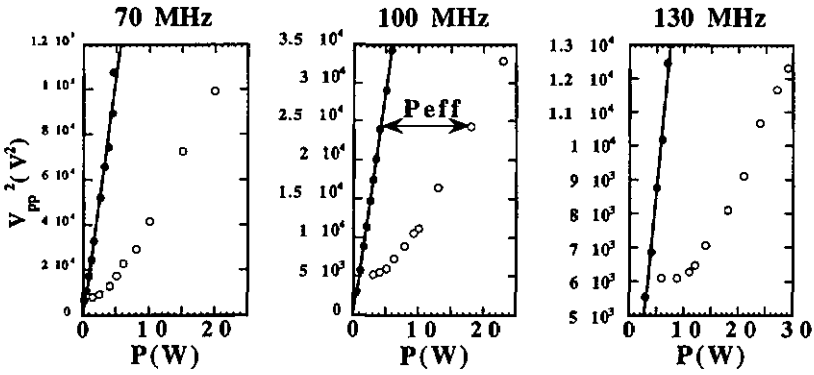

Fig. 4.10a. Evaluation of the effective power coupled to the plasma (Peff) by graphically substracting the network losses (Ploss; full dots) from the total applied power (Pappl; open circles). The measurements were done for 70, 100 and 130 MHz.

It was reported by A.A. Howling et al. [6], that the Vpp - values actually already reach a very low value at 70 MHz. This is consistent with our measurements as sbown in fig. 4.10b, where for very low effective plasma powers we see that the corresponding Vpp-values converge and that a further increase of excitation frequency beyond 70 MHz does not significantly contribute to a substantial decrease of Vpp.

However, as also shown in fig. 4.10b, the situation changes, when always higher effective plasma powers are applied. We observe e.g. that for an effective plasma power of 15 W, an increase of the excitation frequency from 70 MHz up to 130 MHz is simultaneously accompanied by significant reduction of Vpp from about 300 V down to 100 V. This means that the ion impact energy at the substrate is acceptably low even at high effective plasma power levels, if the excitation frequency is high enough. This result is also consistent with the measured lower peak ion energies (together with a higher flux of precursors) for always higher excitation frequencies as shown by M. Heintze [7] and confirms the "soft" nature of the VHF-plasma.

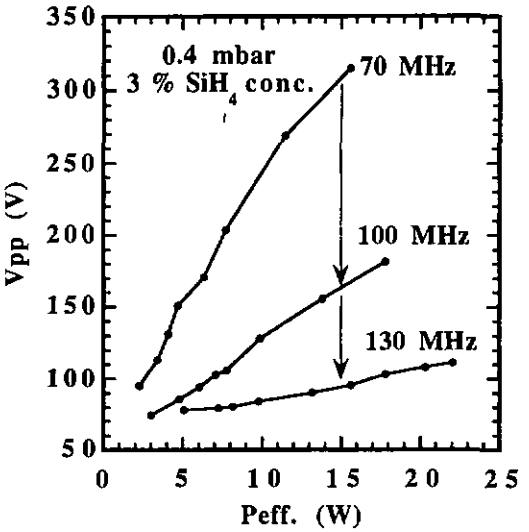

Fig. 4.10b. Measured peak to peak voltage (Vpp) in function of the effective power coupled to the plasma (by applying the substratctive method [10]).

In conclusion, the significantly lower Vpp-values even under higb VHF-power levels at an excitation frequency of 130 MHz motivated us to try a "power" approach for increasing the deposition rate of μc-Si:H.

4.3.2. VHF-power series of μc-Si:H

Basically, we took up the layer from the dilution series shown in the previous section at 5% dilution. In a first step we tried to "fine tune" this layer before increasing, in a second step the applied VHF-power up to 30 W. This 5 % dilution layer was deposited with the highest silane concentration (highest deposition rate) that still has clear X-ray diffraction peaks. However this same layer has been shown to contain a non negligible fraction of amorphous phase. To enhance the crystallinity of this material we took some "technical measures" that are known to improve crystalline growth:

The process pressure has been increased from 0.4 mbar to 0.8 mbar to maintain the plasma confined between the electrodes at the higher power levels investigated here [97].

Additionally, it has been reported by M. Heintze et al. [22] that increasing the process pressure results in a better crystallisation.

An increase of the excitation frequency from 110 MHz to 130 MHz not only reduces the ion impact energy (see fig. 4.10.) but also facilitates the μc-Si:H growth together with higher deposition rates as has been shown by P. Hapke et al. [19, 101]. The same authors even demonstrated that a morphological transition from a-Si:H to μc-Si:H can be achieved by an increase of the excitation frequency with otherwise fixed deposition parameters.

As shown in fig. 4.11. the lowest possible VHF-power that can be applied under these new and improved deposition conditions that still results in a homogeneous filling by the plasma of the interelectrode space is limited to about 9 W. For this power level we already observe an increase of the deposition rate to 3.2 Å/s as compared to the 5 % dilution layer from the dilution series (2.4 Å/s) described in the previous section. A further systematic increase of the VHF-power leads to an almost linear increase of the deposition rate of approximately 0.2 Å/W up to 6.9 Å/s for 30 W.

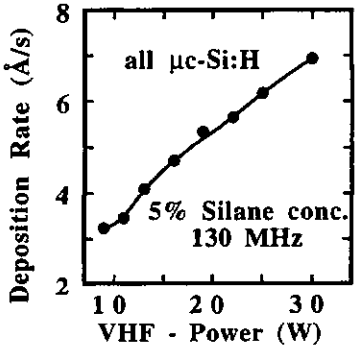

Fig. 4.11. Deposition rate in function of the applied VHF-power at 5 % dilution.

Let us first have a look at the optical properties of these layers as shown in fig. 4.12. Contrary to the very unsatisfying optical absorption properties of the materials obtained in the dilution series (see fig. 4.9.) the apparent optical absorption of all the investigated layers of the present power series all fulfil the requirement of enhanced apparent optical absorption. On one side they all clearly exhibit the desired enhanced apparent optical absorption as compared to c-Si in the region of visible and near IR light. Furthermore, the defect connected absorption is very low for all the layers. However, comparing the measured apparent absorption with the "scattering-free" true absorption evaluated therefrom [49] one realises that the influence of scattering becomes more and more important at always lower photon energies (IR) and clearly dominates in the region of defect connected absorption (around 0.8 eV). Therefore, the defect densities that can be associated to the defect connected absorption represent the uppermost

possible defect density. When we apply the evaluation procedure for the defect density from α proposed by W.B. Jackson et al. [102], we deduce for the 30 W sample with the highest apparent defect-connected absorption ($\alpha \approx 2\,cm^{-1}$ at 0.8 eV) a defect density of about $1 \cdot 10^{16}\,cm^{-3}$. Taking into account the important enhancement of the apparent optical absorption by scattering effects, the true defect density in the 30 W and all the other layers is clearly below this value.

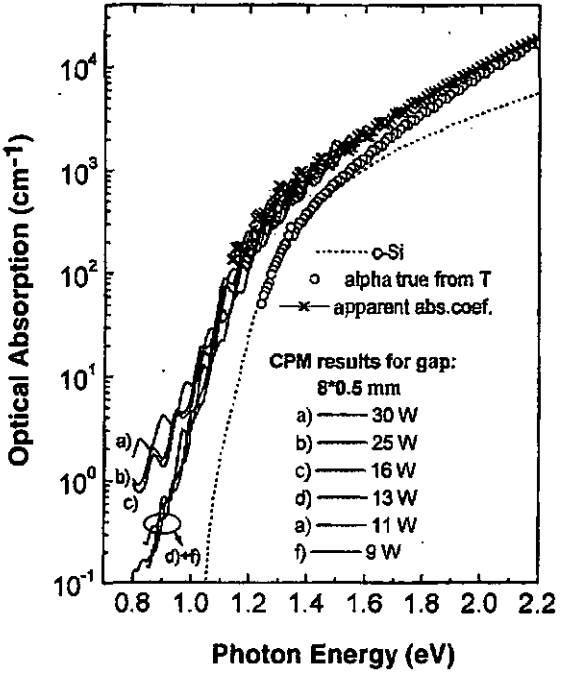

Fig. 4.12. Apparent optical absorption measured by CPM for the 5 % dilution power series.

In agreement with the optical absorption measurements, the X-ray measurements of this power series clearly show that all layers are μc-Si:H (see fig. 4.13.). Furthermore, all the samples have the same diffraction patterns: again, the (220) diffraction peak is dominating over all other peaks, but in contrast to the dilution series, the (220) texture in this power series is so pronounced that the (111) diffraction peak is missing. Note, that such a pronounced (220) texture is also known for polycrystalline silicon deposited by CVD at temperatures between 600 - 650°C [4]. At higher temperatures the [100] orientation predominates, but the structure still contains significant contributions from other orientations, such as (110), (111), (311), and (331).

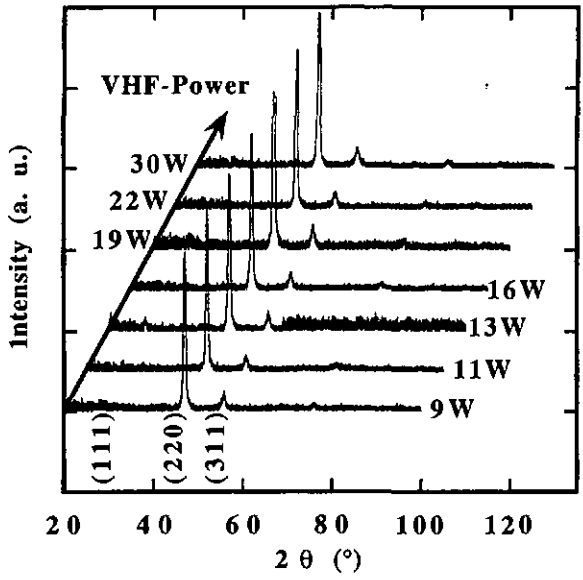

Fig. 4.13. X-ray diffraction spectra for the power series at a dilution of 5 %. A strong 220 texture is evident for all the layers; the [111] - axis is even missing and the [110] - axis is clearly dominant. For our measuring set-up, this means that all (220) planes are parallel to the substrate surface. The spectra are shifted for a better visibility.

The IR-absorption measurements of the power series are shown in fig. 4.14. Again, the observed absorption of the vibrational modes is very similar for all the samples of the series. The calculated hydrogen content ranges from 4 - 6 %, that seems to be enough to efficiently passivate deep defects [59]. Contrary to the X-ray spectra, the IR absorption measurement is sensitive enough to detect slight changes with increasing power. The 2100 cm^{-1} vibrational mode (together with the 626 and 900 cm^{-1} vibrational modes assigned to mono and/or dihydride bonds on (100) and (111) surfaces of crystalline silicon) is continuously growing at the expense of the 2000 cm^{-1} mode, a typical fingerprint of a-Si:H. However, in the dilution series the shift from the a-Si:H related 2000 cm^{-1} vibrational mode to the 2100 cm^{-1} vibrational mode was much more pronounced as that series contained the whole morphological transition from purely amorphous to highly μc-Si:H material. Thus, basically, enhancing the applied VHF-power has a similar effect as increasing the dilution level. However, here the lowest power level already results in μc-Si:H growth and therefore the observed changes are less obvious.

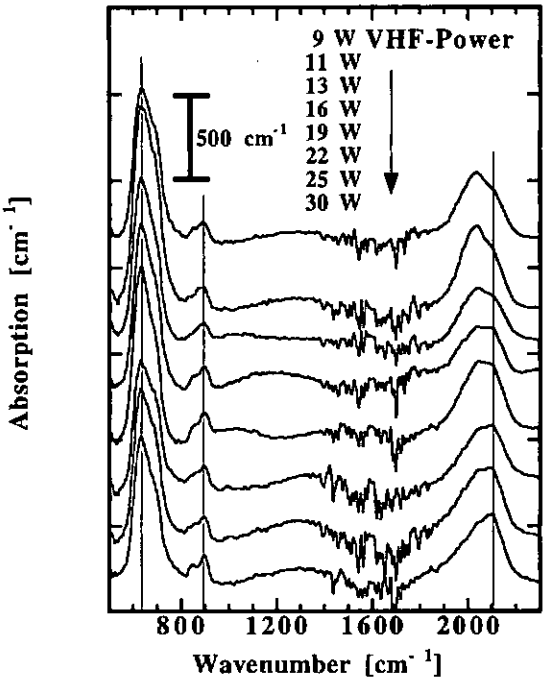

Fig. 4.14. IR - absorption spectra of layers prepared at a fixed dilution of 5 % and at different VHF-power levels. The highlighted vibrational modes can be assigned to mono and/or dihydride bonds on (100) and (111) surfaces of silicon crystallites.

Looking at these results, the most pertinent question is what will happen if we start a similar power experiment with a dilution level that clearly results in amorphous growth under the usual low power conditions?

This issue will be addressed in detail in the next section, where we will increase the silane concentration to 7.5 %. Before stepping further, we wanted to be sure, however, that we are on the right track and that our materials are indeed promising PV - materials. In fact, with our 5 % dilution high power material we already achieved our first target, namely a deposition rate over 5 Å/s.

Without any interface optimisation we directly incorporated the μc-Si:H material deposited with 22 W VHF-power in a n-i-p cell. The cell thickness was 3.6 μm, that corresponds to an i-layer net deposition time of only 1h 45 min (5.7 Å/s) in contrast to 10 h that would be needed for a deposition rate of 1 Å/s.

The spectral response of this cell is represented in fig. 4.15 and shows an almost complete collection without applied reverse voltage. Operating the solar cell even under -4 V reverse voltage shows only a very small increase of the spectral response. Complete spectral response and current - tension characterisation of this solar cell results in a conversion efficiency of 6.5 %.

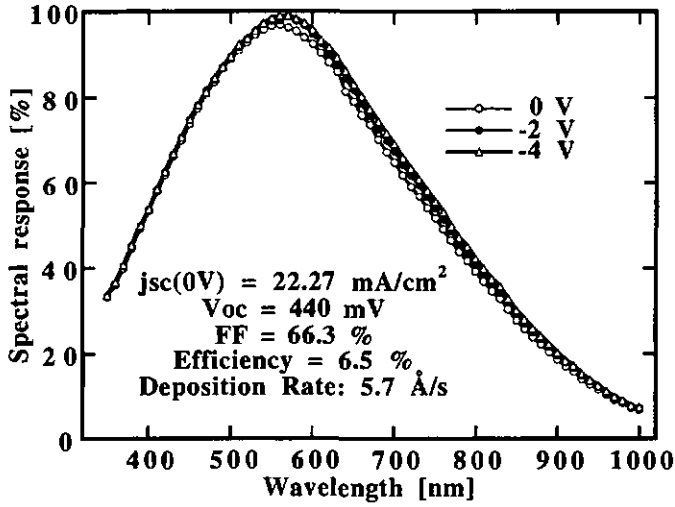

Fig. 4.15. Spectral response of a microcrystalline n-i-p solar cell with a conversion efficiency of 6.5 %. The i-layer deposition rate is 5.7 Å/s, for a thickness of 3.6 μm this corresponds to a net deposition time of 1h 45 min.

This new high power technique was then immediately and successfully applied to opaque substrates (aluminium and stainless steel). The world-wide first n-i-p/n-i-p micromorph tandem solar cell on aluminium (with a deposition rate of 4.3 Å/s for the μc-Si:H layer) was presented in [97, 98]. Recently, a n-i-p/n-i-p micromorph tandem solar cell on stainless steel using the same technology was deposited with a deposition rate for the μc-Si:H bottom cell of even 5.7 Å/s. This cell had a conversion efficiency of 9.25 %, the spectral response is shown hereafter in fig. 4.16.

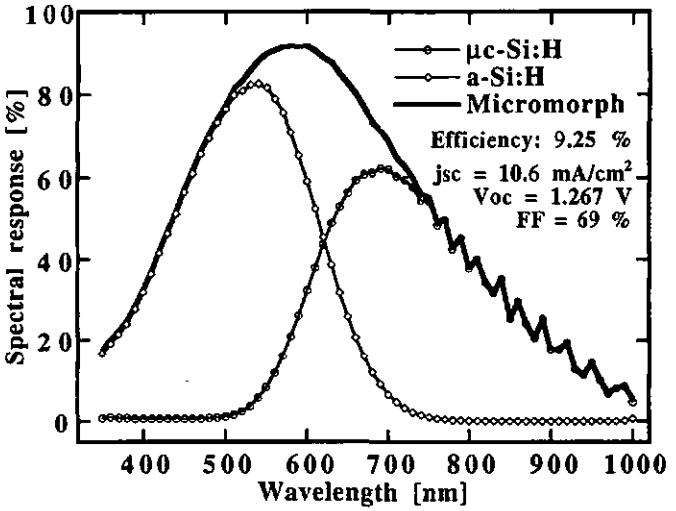

Fig. 4.16. Spectral Response of the first micromorph cell deposited on stainless steel. This tandem cell is very well equilibrated since the spectral response of both cells results in a short circuit current density 10.6 mA/cm^2. Cell conversion efficiency is 9.25 %.

In conclusion we have shown that high deposition rates of μc-Si:H material of device quality can be achieved with the VHF-GD deposition technique by applying relatively high VHF-power levels. Based on our Vpp measurements, we think, however, that this "power approach" was only successful because the ion impact energy under VHF conditions (130 MHz) remains low enough not to create too much defects in the ongrowing crystalline network even at relatively high VHF-power levels. First unoptimised single junction (6.5 % conversion efficiency) and micromorph n-i-p/n-i-p (9.25 % conversion efficiency) produced by this technique confirm the viability of this "power approach".

4.4. VHF-power controlled morphology

In this section we basically intend to take advantage of the results obtained sofar:

First, from the dilution series we learned that by increasing the silane gas phase ratio the deposition rate goes up. However, the gain in deposition rate was apparently on the expense of the desired enhanced optical absorption and, furthermore, we know from previous experiments that at high enough silane concentrations the morphology dumps to amorphous.

Second, we demonstrated that the deposition rate can also be enhanced by increasing the VHF-power level (this time without major losses in material quality).

These two approaches (dilution and power) not only both show a potential to increase the deposition rate, but, furthermore, they show the same trends; more marked for dilution than for power. On the other hand, texture could be modified mostly with changes of power. This observation may suggest that dilution and VHF-power have an equivalent effect on the morphology. A similar result has been shown by Matsuda in 1983 [50]. He demoastrated for standard PECVD (13.56 MHz plasma excitation frequency) that pronounced hydrogen-dilution alone is not a necessary condition for μc-Si:H growth: for a given hydrogen-dilution of silane high enough RF-power levels also yield to μc-Si:H growth. However, deposition rates remained here below 1.5 Å/s.

Choosing now a high silane concentration of 7.5 % in the source gas (that is not sufficient even under standard low power VHF-conditions to allow μc-Si:H growth) we want to force notwithstanding the morphological transition to μc-Si:H by feeding really high VHF-power levels into the plasma. By this experiment, we expect to start with growing an amorphous layer at already quite high deposition rate and, by turning up the VHF-power, to push the μc-Si:H deposition rate to a maximum. We thereby expect to take advantage of the VHF-technique and further of the combined potential of both, high silane concentration and high power for fast growth of μc-Si:H.

To this end we used the identical deposition parameters of the former 5 % VHF-power series (pressurre, temperature, excitation frequency). We then increased the silane concentration to 7.5 % and raised the VHF-power from 20 up to 70 W [103, 104].

In fig. 4.17 the X-ray diffraction patterns of the films prepared at the fixed dilution of 7.5 % are shown as a function of the applied VHF - power. At 20 W the absence of diffraction peaks reveals the growth of a-Si:H. At higher VHF-power levels crystallites can be detected: the main diffraction peaks that can be observed are those for the (111), (220) and (311) planes. For convenience, we have plotted in fig. 4.18 the ratio of intensities of the (111) and (220) peaks. Again, we observe a strong (220) texture with a maximum at 50 W that is even more pronounced than in the (low power) dilution series. On the other side, in contrast to the

5 % power series where the (111) diffraction peak was missing, the latter is clearly visible for all the μc-Si:H layers here.

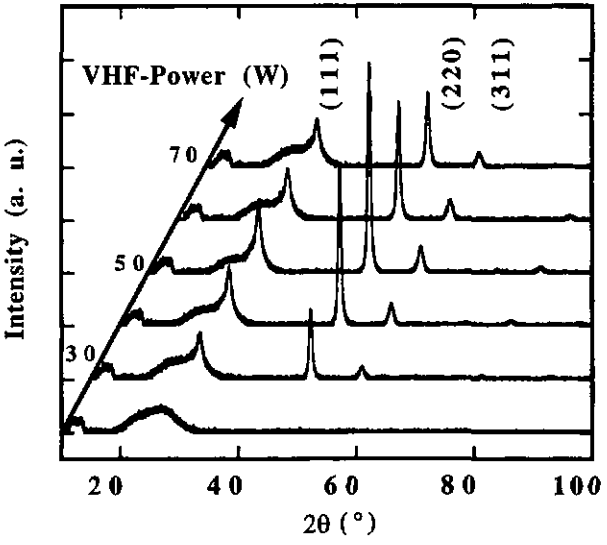

Fig. 4.17. X-ray diffraction pattern of layers deposited at a fixed dilution of 7.5 %. At a low VHF-power level of 20 W the morphology is amorphous, but at higher VHF-power we can clearly see an onset of crystalline growth.

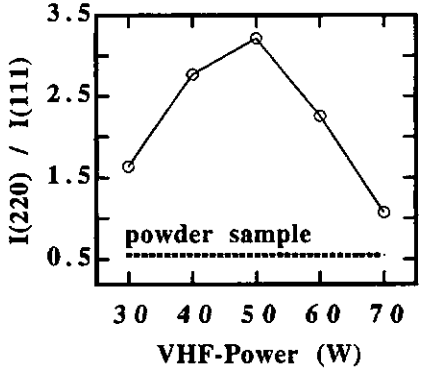

Fig. 4.18. Texture of the 7.5% power series. All samples show a clear preferential growth along the [110] axis with a clear maximum at 50 W VHF-power when compared to the silicon powder sample, where the I(220)/I(111) ratio is 55 %.

The IR - absorption measurements show a similar picture. Typical "fingerprint" patterns at 640, 840, 880 2000 and 2090 cm^{-1} pertaining to the bonding structure of a-Si:H can mainly be seen for the 20 W sample and become smaller and even disappear when going to higher VHF-power levels. At the same time, the characteristic peaks of for μc-Si:H at 626, 900 and 2100 cm-1 attributed to mono/dihydride bonds on (100) and (111) surfaces of crystalline surfaces arise at higher VHF - power levels. The bonded hydrogen content is evaluated to be between 5 - 10 % for the μc-Si:H samples. This is slightly higher than in the previous series.

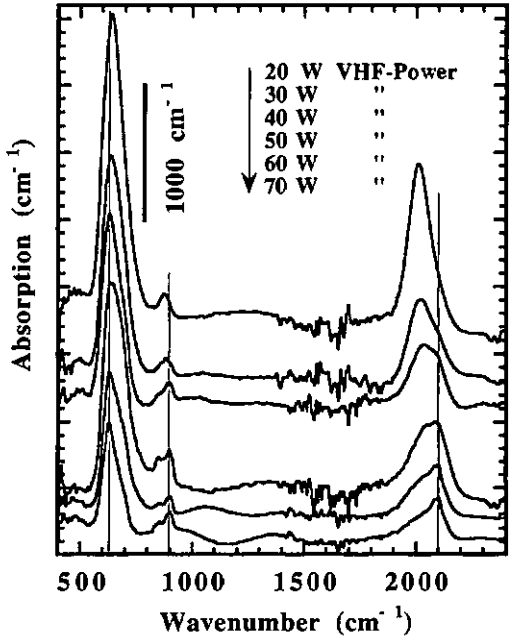

Fig. 4.19. IR-absorption spectra of layers prepared at different VHF-power levels as indicated in the figure. The spectra are shifted vertically for clarity. The fine vertical lines point to the absorption around 626, 900 and 2100 cm^{-1} which can be associated to modes from mono/dihydride bonds on crystallite surfaces.

In other terms, we observe a similar behaviour as in the dilution and power series, starting however this time from amorphous material and covering the whole morphological

transition. Thus, it seems that high hydrogen dilution can, indeed, be replaced by substantially enhanced VHF-power levels.

In fig. 4.20 we reported the (220)/(111) X-ray diffraction ratio as well as the IR - absorption at 2100 cm^{-1} as a function of the VHF - power. Apparently the (220) texture is correlated with the appearance of mono/dihydride bonds on (100)/(111) surfaces of silicon crystallites (IR - absorption around 2100 cm^{-1}). This is interesting in the context of the surface passivation properties that hydrogen shows on silicon [57, 58]. One may indeed raise the question whether we have here crystallites arranged vertically along the [110] axis with surrounding surfaces (i.e. grain boundaries) where bonded hydrogen passivates dangling bonds.

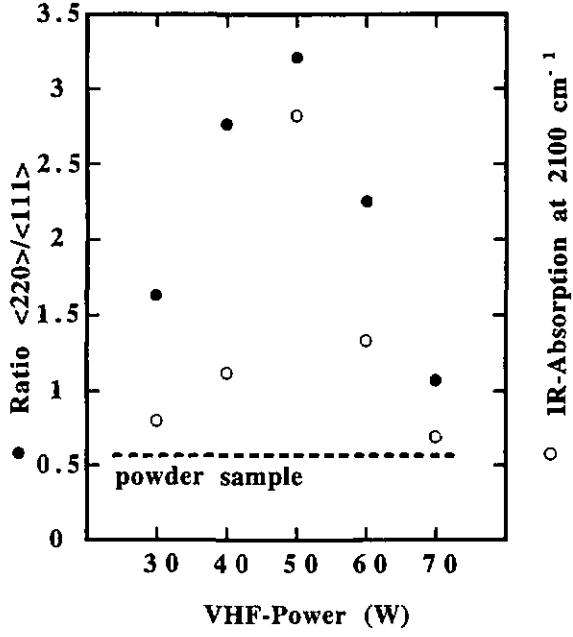

Fig. 4.20. Ratio of the (220)/(111) X-ray diffraction peaks for a silicon powder sample with random orientation and for the series presented here. Preferential growth along the [110] axis is evident for all the layers, with a clear maximum around 50 W. IR-absorption at 2100 cm^{-1} is also shown (stretching modes around 2100 cm^{-1} can be assigned to mono/dihydride bonds on (100) / (111) surfaces of silicon crystallites).

The optical absorption plotted in fig. 4.21 measured by PDS shows consistently with IR and X-ray measurements the occurence of a morphological transition: the 20 W material is

purely amorphous whereas all the other layers show same crystalline-like absorption. The defect - connected absorption at around 0.8 eV is similar for all μc-Si:H samples. However, one has to keep in mind that scattering related enhancement of the optical absorption as well as the detection limit of the PDS technique [59] in this low absorption region renders a more quantitative evaluation of the defect density difficult. The only message that can be directly drawn therefrom is the utmost possible defect density of still reasonable $3 \cdot 10^{16}$ cm^{-3} for all these μc-Si:H layers. A scattering-corrected evaluation of the defect density for the 40 W sample shows, indeed, that the effective defect density is substantially lower, i.e. about one order of magnitude ($3 \cdot 10^{15}$ cm^{-1}).

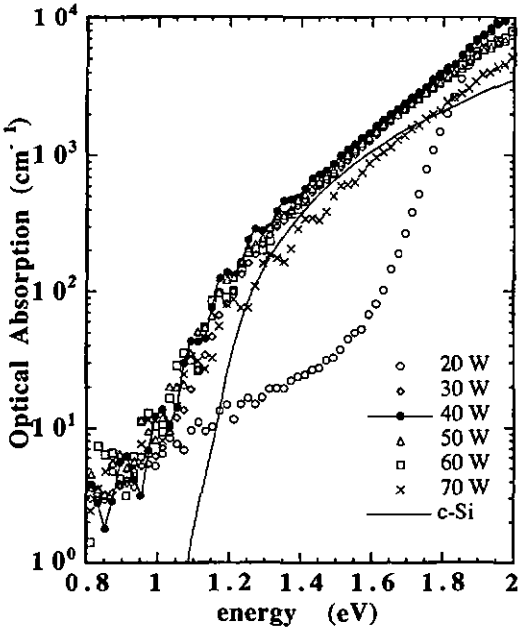

Fig. 4.21. Optical absorption as measured by PDS for the VHF - power series at 7.5 % dilution.

Looking now at the measured optical absorption of the μc-Si:H materials (30 W and higher) in the region around 1.4 eV, another interesting feature can be seen: even though all these layers are clearly microcrystalline from the structural measurements, they show variations in the optical absorption of about a factor of 2. In contrast to the "high" energy

region ($E > 1.8$ eV or $\lambda < 690$ nm) where the absorption of μc-Si:H ($\alpha \geq 5 \cdot 10^3$ cm^{-1}) suffices in a solar cell with 3.6 μm thickness to absorb at least 90 % of the incoming light in a single optical path this doesn't hold for photons of lower energies. In the spectral region around 1.4 eV (886 nm) the situation is becoming more critical: at this energy, e.g. a 2 times higher apparent optical absorption of the material immediately allows the reduction of the cell thickness by the same factor while still absorbing the same amount of sunlight.

At this level the question must be risen, where these changes in absorption come from. As a first hand explanation, one may speculate that variations in the crystalline volume fraction that are not visible by IR or X-ray measurements, may occur. To check this possibility, we performed Raman-measurements in order to determine the crystalline volume fraction in this particular series. The result, plotted in fig. 4.22, is evident: the crystalline volume fraction is constantly high for all μc-Si:H materials and can therefore not account for the observed variation in the optical absorption around 1.4 eV (see also fig. 4.23.).

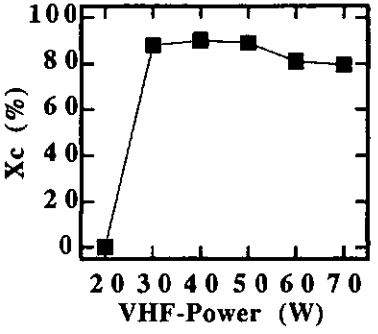

Fig. 4.22. Crystalline volume fraction as determined from Raman spectra.

Another possible explanation would be scattering-related enhancement of the optical absorption due to the surface roughness of the layers. To this end we determined the rms surface roughness by a surface profilometer (α - step Tencor) and plotted the results together with the apparent optical absorption measured at 1.4 eV (see fig. 4.23.). The correlation between apparent α and the surface roughness becomes quite evident from this picture and we therefrom conclude that the changes in optical absorption are mainly due to surface scattering [105].

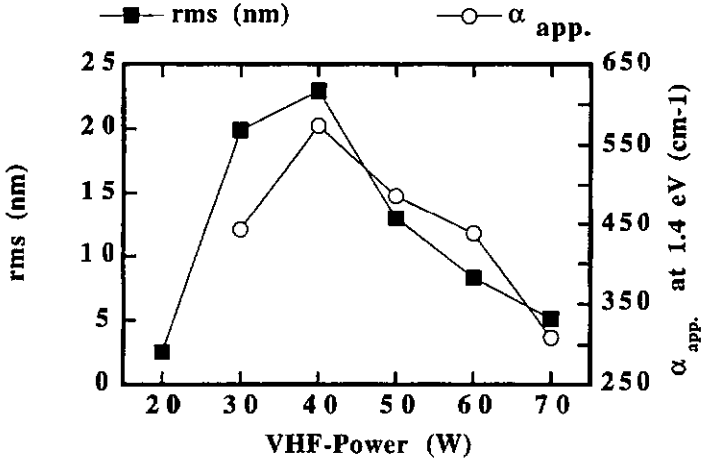

Fig. 4.23. rms surface rougbness and optical absorption at an energy of 1.4 eV for the VHF-power series at a dilution of 7.5 %.

After this detailed material characterisation we were motivated to investigate how this new 7.5 % VHF - power series of μc-Si:H layers perform within the device. We therefore deposited n-i-p solar cell diodes incorporating these layers as absorbing i-layers to actually check their performance.

In fig. 4.24. we show deposition rates thereby obtained. A steady increase of the deposition rate is observed by increasing the applied VHF-power. Unusually high deposition rates up to 13 Å/s for μc-Si:H material are observed and reflect the synergetic effect of both a high silane gas phase ratio and a high VHF-power level.

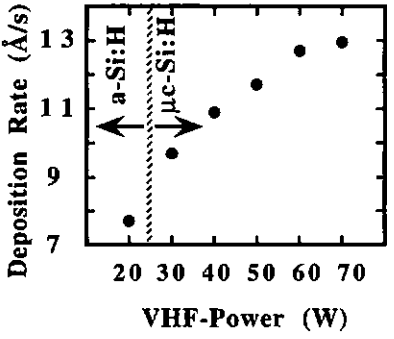

Fig. 4.24. Deposition rate of n-i-p solar cells in function of the applied VHF-power.

Note that for the lowest VHF–power resulting in μc-Si:H growth (30 W) in the present 7.5 % series the deposition rate exceeds the highest deposition rate obtained in the previous power - series at 5 % dilution. At the same time, the initially set target of 10 Å/s is achieved for all the other μc-Si:H materials of this series.

In fig. 4.25a, b performances of the n-i-p solar cells are given. Note that the structure employed has a specific advantage when growing fully μc-Si:H solar cells. The thin window layer (p - type μc-Si:H) has a strong tendency to pick up the underlying morphology and, thus nucleates rather bad on a-Si:H [106]. This can also be seen in the low spectral response at short wavelength for the 20 W a-Si:H cell indicating a serious problem with this p-layer (see fig. 4.26.). Surprisingly, a similar but less drastic effect is also visible for the cell incorporating the 30 W i-layer. This could also explain the increase in fill factor (FF) for higher VHF-power levels, since nucleation is facilitated (on μc-Si:H). Furthermore, in fig. 25a, a continuous decrease in V_{OC} is observed for the cells deposited at increasing power and can to some extend be explained by the decrease of the optical gap of the corresponding materials.

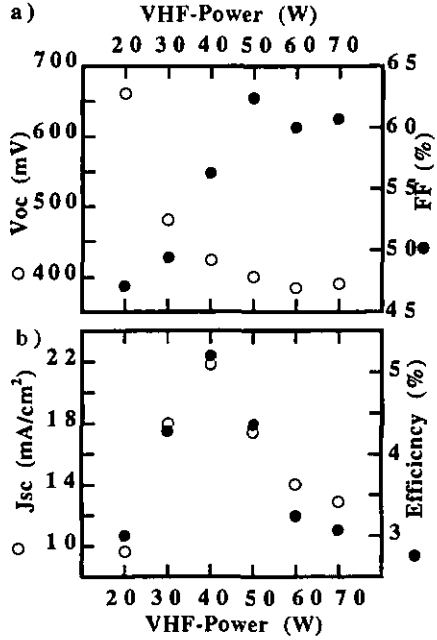

Fig. 25a, b. n-i-p solar cell performances after direct implementation of the i-layers which morphology is controlled by the VHF-power only.

The strongest effect of μc-Si:H growth and structure on the solar cell performance can be observed for the short circuit current density. For this particular series, the highest obtained conversion efficiency is 5.2 % at a deposition rate of 10.9 Å/s (jsc = 21.8 mA/cm^2, FF = 56 %, Voc = 424 mV).

In fact, the obtained cell conversion efficiencies are well correlated with the short circuit current density (fig. 4.25b) and reflects mainly the changes in the optical absorption of the incorporated material as will be shown hereafter.

In fig. 4.26. the spectral response measurements of the entire 7.5 % power cell series are plotted. For the μc-Si:H cells we observe the gap related extended spectral response to the red as compared to the a-Si:H cell (20 W). Furthermore, within the μc-Si:H solar cells, a steady decrease of the red spectral response with increasing power is observed. As shown in the following fig 4.27. this reduced spectral response can be associated to a large extent to the decreasing optical absorption of the μc-Si:H materials deposited at increasing power levels. In fact, even though the 70 W μc-Si:H solar cell additionally exhibits a charge collection problem (collection increases with applied reverse bias voltage), it cannot account for the observed substantial differences between the 70 W and 40 W μc-Si:H cells. These observations of spectral response (and thus also short circuit current density and conversion efficiency) are in good agreement with the optical properties measured in the corresponding layers and discussed previously (fig. 4.23.).

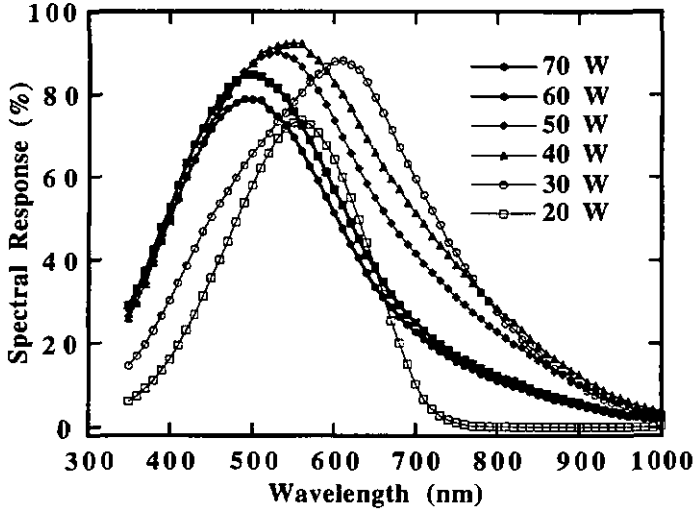

Fig. 4.26. Spectral response for cells incorporating the VHF-power series at a dilution of 7.5 %.

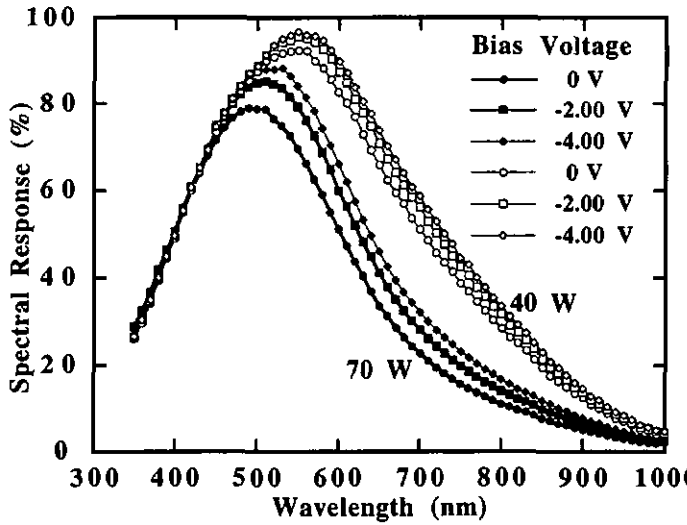

Fig. 4.27. Spectral Response under reverse bias voltage for the cells incorporating the 40 and the 70 W layer respectively. Comparison of the measurements performed at -4 V reveals that the difference in the red spectral response is mainly due to differences in the optical absorption.

As far as charge collection is concerned, the present unoptimised (!) cells incorporating the 7.5 % power series still bear the potential of further improvement. Two different ways may be followed up: first, the process parameters for deposition should be further optimised (deposition temperature, interfaces, contacts, light trapping, anti-reflecting coatings, etc.) towards higher cell conversion efficiencies, second it would also be desirable to have a characterisation method (like for a-Si:H [107]) that allows a direct evaluation of the intrinsic material in the device. Efforts in this direction are in progress [108].

4. 5. Optical emission spectroscopy

The forth state of matter, the plasma phase, consists of an ensemble of free electrons, neutrals and ions. Under the VHF-GD conditions used, reactive species are mostly due to the electron impact onto the molecular source gases (SiH_4 and H_2). These reactive species condense on the nearby substrate forming thereby the coating. The necessary energy to dissociate and / or excite the molecules of the source gas is supplied at the base by the applied VHF-power. Free, highly mobile electrons accelerated by the applied VHF-power sustain the plasma - "flame" by impact ionisation: thereby positive ions and free electrons are created. Few electrons may be sufficient to ignite the plasma. Involved plasma reactions and interactions are of a rather complex nature, there is no consistent picture available yet (see e.g. [109]). However, among the light emitted from the plasma some intense line emission can be observed. They result form discrete energy transitions from a formerly excited level down to an intermediate or the ground level. These transitions accompanied by emission of photons are direct accessible fingerprint patterns and give insight in the involved reaction species as well as may clarify reaction mechanisms.

Optical emission spectroscopy (OES) is a quite simple in-situ characterisation technique which does not disturb the plasma. In our case it consists of decomposing the light emitted from the plasma with a monochromator and spectrally detecting the intensity with a photodiode at the exit slit (see fig. 4.28.).

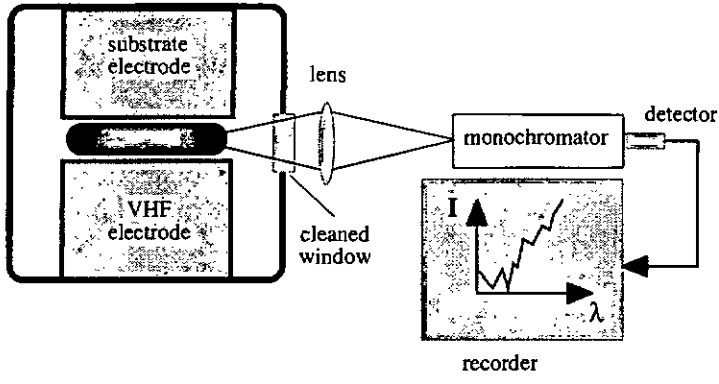

Fig. 4.28. Experimental set-up for measuring the optical emission spectroscopy (OES).

Special care was taken to check whether the chamber window was covered by a layer during deposition, since otherwise a transmittance loss mainly in the UV-region could give misleading measurements. For this particular set-up (reactor, monochromator, detector) a spectrum recorded under precisely known deposition conditions may be used later as a calibration or for ulterior comparisons. However, since no absolute calibration of the spectra is done, comparisons to other systems can only be done on a relative basis.

Fig. 4.28. shows typical OES as obtained with our set-up, for deposition conditions of low VHF-power level (6 W) in function of the hydrogen-dilution of silane. The spectral lines of main interest which will be considered hereafter are situated at 414 and 656 nm. The former line is associated to the SiH* radical and the latter to atomic hydrogen H_α. These lines of our interest are marked in the same fig. 4.28. and we will analyse how they evolve by changing the process parameters. As can further be seen in fig. 4.28 there are more well visible lines that will however not be further considered here, as e. g. the lines around 603 nm, the so called Fulchner - lines, which correspond to transitions withio molecular hydrogen, etc.

As shown by Mishima et al. in 1982 [110] it is possible to correlate the morphological transition from amorphous to microcrystalline silicon to the SiH*/Hα ratio, i.e. beyond a certain SiH*/Hα ratio the morphology of the grown film is strictly μc-Si:H. This relation has also been observed by Matsuda in 1983 [50]. Further, in all these works done at the standard rf-PECVD at 13.56 MHz, deposition rates scale fairly well with the SiH* - line. Later, Oda et al. [111, 112] compared the OES of standard rf-PECVD at 13.56 MHz with the OES of VHF - PECVD at an excitation frequency of 144 MHz. Consistently similar results have been found for the morphological transition, however with a focus mainly to explain higher deposition rates of a-Si:H under VHF conditions. Nevertheless, with the help of such OES measurements a broader process window under VHF-conditions for the growth of μc-Si:H could be brought already then to evidence.

Thus, we performed OES for two selected series [113] where the morphological transition has been controlled by varying one parameter alone; the first series is the dilution series as presented in section 4.2. and the second series is the VHF-power series as shown in section 4.4.

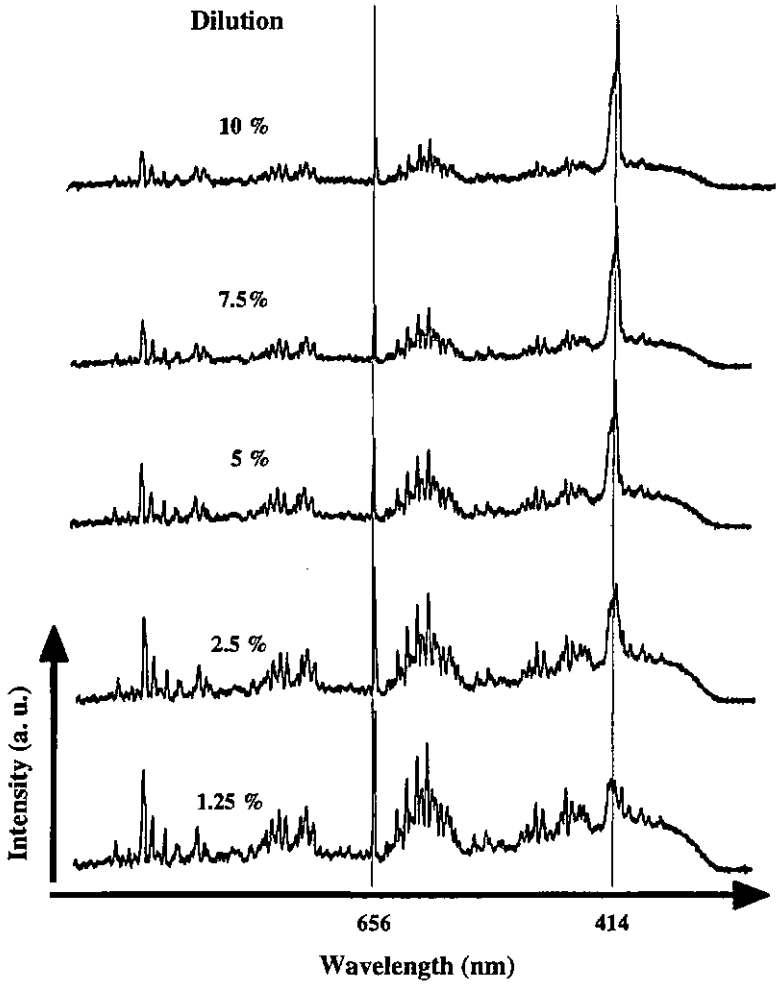

Fig. 4.28. Optical Emission Spectroscopy (OES) as obtained in our set-up for the dilution series under VHF-GD conditions. The lines of our interest are situated at 414 and 656 nm and correspond respectively to the SiH* radical and to atomic hydrogen (H_α).

Fig. 4.29. shows the SiH* and the Hα lines versus the silane gas flow concentration employed for their deposition. Note that the morphology changes from μc-Si:H to a-Si:H when the dilution level is changed from 5 to 7.5 %, according to the X-ray measurements (fig. 4.6.). In agreement with observations previously reported in the literature, μc-Si:H

growth is observed as soon as enough atomic hydrogen is available. This can be seen in fig 4.29. where samples with the lowest silane concentration of 1.25 to 5 % exhibit also the lowest SiH*/Hα ratio. On the other hand, if the SiH*/Hα ratio is high, the obtained layer is a-Si:H (as is the case for the samples deposited at a silane gas phase ratio of 7.5 and 10 %).

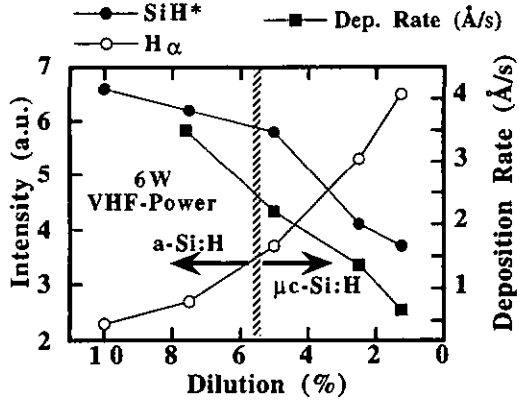

Fig. 4.29. OES for the SiH* and Hα lines for a dilution controlled morphological transition. As soon as enough atomic hydrogen (Hα) is available w.r.t. the SiH* radical, the morphology becomes μc-Si:H. Further, the deposition rate scales with the SiH* line.

The same measurement is shown for the VHF-power controlled morphological transition in fig. 4.30. (at a fixed gas phase ratio of 7.5 % silane). Increasing the VHF - power leads to a continuous decrease of the SiH*/Hα ratio and also here we can find μc-Si:H growth when this ratio is low enough. Furthermore, owing to much higher plasma densities all the measured OES intensities are shifted to much higher values (the arbitrary units on the y-axis are the same in both figures); the overall emitted intensities are increased by about a factor of five and reflect much higher dissociation rates in the plasma. This increased dissociation rate explains probably the approximately 5 times higher deposition rates as observed for all the samples (whether a-Si:H or μc-Si:H) of this power series compared with the dilution series. Further, as can be seen in figs. 4.29. and 4.30, the deposition rate scales with the intensity of the SiH* - line for both, the dilution and the VHF power series. This has also been shown by [6] for the growth of a-Si:H under VHF-conditions.

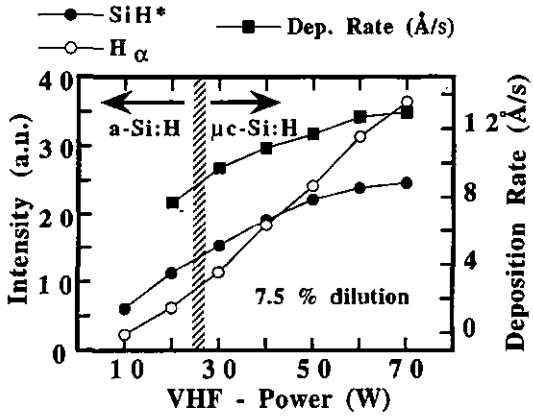

Fig. 4.30. OES for the SiH* and Hα lines for the morphological transition as controlled by the VHF-power. Also here, as soon as enough atomic hydrogen w.r.t. the SiH* radical is available, μc-Si:H growth is obtained. The deposition rate increases also with the SiH* line.

In both the dilution and in the VHF-power series, process parameters can be chosen by monitoring characteristic OES which are known to lead strictly to μc-Si:H growth. This is the case when the SiH*/Hα ratio is below a certain value. Obviously, the opposite is true for a-Si:H growth.

This is further illustrated in fig. 4.31, where on the x-axis the SiH*/Hα ratio is shown for both series: On the left y-axis we can read the silane gas phase ratio employed for the dilution series and on the right y-axis the applied VHF-power for the power series is specified. For the particular measurement set-up used here, we see that when the SiH*/Hα ratio is well below 1.7 we obtain μc-Si:H growth. This fixed ratio which determines the morphology is consistent with literature [50, 110-112, 114] and is a further proof how helpful OES measurements can be to gather new deposition conditions. Even though the two series come from quite different deposition conditions, it is shown that determination of the microstructure of the films is achieved by comparison of the SiH*/Hα ratio. Keeping in mind that μc-Si:H growth is achieved for the dilution series at a deposited rates only below 2.5 Å/s, the VHF-power series attains within the μc-Si:H growth regime deposition rates well above 10 Å/s. To the best of our knowledge, these are the highest deposition rates using glow discharge for device quality μc-Si:H that have been reported to the date of writing of this work. It is evidenced from these OES studies, that the "plasma chemistry" remains essentially the same for achieving μc-Si:H at high rates, though the overall intensity of OES is shifted to much higher values.

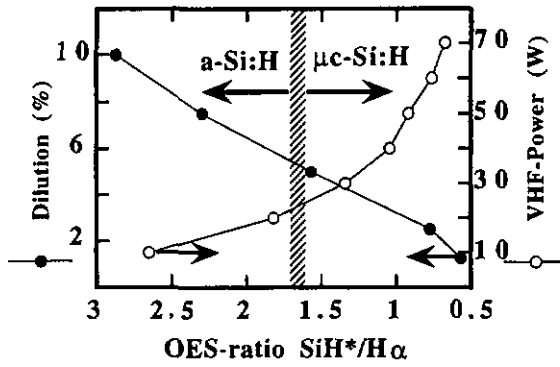

Fig. 4.31. OES for the SiH*/Hα ratio for both the dilution and VHF-power series. On the left axis we can read the employed silane gas phase ratio and on the right axis the applied VHF-Power. As soon as the OES - ratio falls below 1.7 in our particular set-up, we have μc-Si:H growth.

In conclusion, OES is a powerful tool for monitoring the influence of plasma parameters. Even though the two series investigated here by OES come from quite different deposition conditions, it is shown that the SiH*/Hα ratio is a powerful parameter to determine the microstructure of the deposited film. It is observed that the emissions of the SiH* line scales with the deposition rate independently of the obtained morphology of the layers. Thus, OES is an efficient and easy to handle in-situ tool that can certainly contribute to monitor deposition processes.

4. 6. Conclusions

In conclusion, we have proved that it is, indeed, possible to deposit device grade μc-Si:H at substantially higher deposition rates (i.e. ≥ 10 Å/s) thanks to the "soft" nature (low ion bombardment) of the VHF-GD technique (130 MHz). In fact, by taking advantage of restricted hydrogen dilution of silane together with unusually high VHF-power levels we succeeded to grow μc-Si:H with a high crystalline volume fraction (> 80 %) at a deposition rate of 13 Å/s. Fast deposited (10.9 Å/s) n-i-p solar cells achieved so far an (unoptimised) conversion efficiency of 5.2 %. In addition, we have shown that OES can be used as an efficient tool to monitor process parameters in view of the morphology and deposition rate of the ongrowing layer.

V. Final Conclusions

Already now μc-Si:H is one of the most competitive PV materials for the challenge of the next generation of thin-film silicon solar cells. In combination with amorphous silicon within the micromorph concept, μc-Si:H bears the potential for low-cost, large area high efficiency solar cells.

In this thesis work we presented some solutions to three key issues related to μc-Si:H solar cells that hindered so far a fast and successful spreading of this new material:

It has been difficult so far to grow midgap μc-Si:H as needed for an active absorber material in PV applications. We have shown that in our μc-Si:H material the detrimental n-type character is related to oxygen impurities. As a consequence we were able to overcome the previous difficult to bandle "microdoping approach": we successfully reduced and controlled the oxygen contamination in our μc-Si:H material by using the purifier technique. This new approach allowed us to achieve the growth of intrinsic μc-Si:H without needing impurity compensation.

We have also shown that VHF-GD has inherent advantages for the growth of μc-Si:H. Experimentally this was evidenced by low temperature p-type epitaxial growth (at 170°C) and the demonstration of an enlarged parameter space for boron-doped p-type μc-Si:H window layers with increasing plasma excitation frequencies (up to 130 MHz). The "soft" nature (low ion bombardment) of high frequency plasmas was furtber evidenced by $V_{peak\text{-}peak}$ measurements. Finally, we showed that for high enough excitation frequencies the VHF power levels can be increased substantially without inducing a detrimental increase of defects.

Motivated by these results we finally attached ourselves to the solution of one of the major drawbacks of μc-Si:H for a potential industrial production, namely its very low deposition rate of typically ≤ 1 Å/s. We achieved a 10-fold enhancement of the deposition rate by combining the beneficial effects of restricted dilution and high VHF power levels. These fast deposited μc-Si:H materials (10.9 Å/s) were also successfully implemented into first (unoptimised) n-i-p solar cells with a conversion efficiency of 5.2 %.

VI. REFERENCES

1. S. Veprek and V. Marecek, "The Preparation of Thin Layers of Ge and Si by Chemical Hydrogen Plasma Transport", *Solid-State El.* **11**, 683-684 (1968)
2. S. Veprek and M.G.J. Veprek-Heijman, "Open Questions Regarding the Mechanism of Plasma-Induced Deposition of Silicon", *Plasma Chemistry and Plasma Processing* **11**, 323-334 (1991)
3. S. Veprek, M. Heintze, F.-A. Sarott, M. Jurcik-Rajman, and P. Willmott, "Mechanisms of Plasma Induced Silicon Deposition and the Control of the Deposit", *Mat. Res. Soc. Symp. Proc.* **118**, 3-16 (1988)
4. S.M. Sze, *VLSI Technology*, 2 ed., M. Graw-Hill, 1988, ISBN 0-07-100347-9
5. H. Curtins, N. Wyrsch, and A. Shah, "High-Rate Deposition of Amorphous Hydrogenated Silicon: Effect of Plasma Excitation Frequency", *Electron. Lett.* **23**, 228-230 (1987)
6. A.A. Howling, J.-L. Dorier, C. Hollenstein, U. Kroll, and F. Finger, "Frequency Effects in Silane Plasmas for Plasma Enhanced Chemical Vapour Deposition", *J. Vac. Sci. Technol. A* **10**, 1080 (1992)
7. M. Heintze and R. Zedlitz, "VHF Plasma Deposition For Thin-Film Solar Cells", *Pr. in PV: R. and Appl.* **1**, 213-224 (1993)
8. U. Kroll, A. Shah, H. Keppner, J. Meier, P. Torres, and D. Fischer, "Potential of VHF-plasmas for low-cost production of a-Si:H solar cells", *Solar Energy Materials and Solar Cells* **48**, 343-350 (1997)
9. U.J. Kroll, "VHF-Plasmaabscheidung von amorphem Silizium: Einfluss der Anregungsfrequenz, der Reaktorgestaltung sowie Schichteignschaften", *Ph. D. Thesis*, Institut de Microtechnique, Université de Neuchâtel, Neuchâtel, 1994, ISBN 3-89191-905-0
10. V.A. Godyack and R.B. Piejack, *J. Vac. Sci. Technol. A* **8** (5), 3833 (1990)
11. H. Keppner, U. Kroll, P. Torres, J. Meier, D. Fischer, M. Goetz, R. Tscharner, and A. Shah, "Scope of VHF plasma Deposition for Thin-Film Silicon Solar Cells" in *25th IEEE PVSEC* Washington, 669 (1996)
12. P. Torres, J. Meier, R. Flückiger, H. Keppner, and A. Shah, "Enlarged Parameter Space by Use of the VHF-GD for Deposition of Thin p-type μc-Si:H Films", *Mat. Res. Soc. Symp. Proc.* **453**, 767-772 (1997)
13. R. Flückiger, J. Meier, G. Crovini, F. Demichelis, F. Giorgis, C.F. Pirri, E. Tresso, J. Pohl, V. Rigato, S. Zandolin, and F. Caccavale, "Structural and Electrical Properties

of Undoped Microcrystalline Silicon Grown by 70 MHz and 13.56 MHz PECVD", *Mat. Res. Soc. Symp. Proc.* 358, 751-756 (1995)

14. R. Flückiger, J. Meier, H. Keppner, M. Goetz, and A. Shah, "Preparation of Undoped and Doped Microcrystalline Silicon (μc-Si:H) by VHF-GD for p-i-n Solar Cells", in *23rd IEEE Photovoltaic Specialists Conference* Louisville, 839-844 (1993)
15. R. Flückiger, J. Meier, A. Shah, J. Pohl, M. Tzolov, and R. Carius, "Structural, Optical and Electrical Properties if <p> μc-SiC:H Thin Films Deposited By The VHF-GD", in Mat. Res. Soc. Research Society Symposium Proceedings 358, (1994)
16. S. Gosh, A. De, S. Ray, and A.K. Barua, *J. Appl. Phys.* **71**, 5205 (1992)
17. J.-S. Chou, W.-J. Sah, S.-C. Lee, T.-C. Chang, and J.-C. Wang, *Mat. Chemistry and Physics* 32, 273 (1992)
18. K. Prasad, "Microcrystalline Silicon (μc-Si:H) prepared with Very High Frequency Glow Discharge (VHF-GD) Process", *Ph. D. Thesis*, Institut de Microtechnique, Institut de Microtechnique de l'Université de Neuchâtel, Neuchâtel, 1991,
19. F. Finger, P. Hapke, M. Luysberg, R. Carius, H. Wagner, and M. Scheib, "Improvement of Grain Size and Deposition Rate of Microcrystalline Silicon by Use of VHF-GD", *Appl. Phys. Lett.* **65**, 2558 (1994)
20. R. Flückiger, "Microcrystalline Silicon Thin Films Deposited by VHF Plasmas for Solar Cell Applications", *Ph. D. Thesis*, Institut de Microtechique, Université de Neuchâtel, Neuchâtel, 1995, ISBN 3-89191-965-4
21. R. Flückiger, J. Meier, A. Shah, A. Catana, M. Brunel, H.V. Nguyen, R.W. Collins, and R. Carius, "Structural, Optical and Electrical Properties of <p> μc-Si:H Very Thin Films Deposited by the VHF-GD Technique", in *Material Research Society Symposium Proceedings* **336**, 511-516, San Francisco, (1994)
22. M. Heintze and M. Schmitt, "Highly Conductive p-type Microcrystalline Silicon Thin Films", in *Material Research Society Symposium Proceedings* San Francisco, (1996)
23. Y. Hamakawa, Y. Matsumoto, G. Hirata, and H. Okamoto, *Mat. Res. Soc. Symp. Proc.* **164**, 291 (1989)
24. T. Sawada, N. Terada, S. Tsuge, T. Baba, T. Takahama, K. Wakisaka, S. Tsuda, and S. Nakano, in *24th IEEE Photovoltaic Specialists Conference*, 1219 (1994)
25. H. Keppner, P. Torres, R. Flückiger, J. Meier, A. Shah, C. Fortmann, P. Fath, G. Willeke, K. Happle, and H. Kiess, "Passivation Properties of amorphous and microcrystalline silicon layers deposited by VHF-GD for crystalline silicon solar cells", *Solar Energy Materials and Solar Cells* **34**, 201-209 (1994)
26. P. Torres, R. Flückiger, J. Meier, H. Keppner, U. Kroll, V. Shklover, and A. Shah, "Very Low Temperature Epitaxial Growth of <p>-type Silicon for Solar Cells", in *13th EC PVSEC* Nice, 1638-1641 (1995)

27. T. Oshima, M. Sano, A. Yamada, M. Konagai, and K. Takahashi, "Effects of SiH2Cl2 on low-temperature (<200°C) Si epitaxy by photochemical vapor deposition", *Applied Surface Science* 79/80, 215-219 (1994)
28. H. Shirai, H. Tanabe, T. Uemtsu, J. Hanna, and I. Shimizu, "Growth of Amorphous, Microcrystalline and Epitaxial Silicon at the Same Substrate Temperature Under Control of Atomic Hydrogen", *J. of Non-Cryst. Solids* **114**, 810-812 (1989)
29. D.J. Eaglesham, "Semiconductor molecular-beam epitaxy at low temperatures", *J. Appl. Phys.* 77, 3597-3617 (1995)
30. H. Akazawa and Y. Utsumi, "Reaction Kinetics in synchrotron-radiation-excited Si epitaxy with disilane: I. Atomic layer epitaxy, II. Photochemical-vapor deposition", *J. Appl. Phys.* 78, 2725-2750 (1995)
31. G.F. Feng, M. Katiyar, N. Maley, and J.R. Abelson, "Silicon epitaxy at 230°C by reactive dc magnetron sputtering and its in situ ellipsometry monitoring", *Appl. Phys. Lett.* 59, 330-332 (1991)
32. T. Ohmi, K. Matsudo, T. Shibata, T. Ichikawa, and H. Iwabuchi, "Very-Low-Temperature Epitaxial Silicon Growth by Low-Kinetic-Energy Particle Bombardment", in *20th Int. Conf. on Solid State Devices and Materials* Tokyo, 49-52 (1988)
33. W.G. Townsend and M.E. Uddin, "Epitaxial Growth of Silicon from SiH4 in the temperature range 800-1150°C", *Solid-State El.* 16, 39-42 (1973)
34. J.H. Comfort and R. Reif, "Plasma-Enhanced Deposition of High-Quality Epitaxial Silicon at Low Temperatures", *Appl. Phys. Lett.* 51, 2016-2018 (1987)
35. S. Veprek, M. Heintze, F.-A. Sarott, M. Jurcik-Rajman, and P. Willmott, "Mechanisms of Plasma Induced Silicon Deposition and the Control of the Properties of the Deposit", *Mat. Res. Soc. Symp. Proc.* **118**, 3-17 (1988)
36. J.L. Rogers, P.S. Andry, W.J. Varhue, P. McGaughnea, E. Adams, and R. Kontra, "Low-Temperature Homoepitaxial Growth of Si by Electron Cyclotron Resonance Plasma Enhanced Chemical Vapour Deposition", *Appl. Phys. Lett.* 67, 971-973 (1995)
37. S.J. DeBoer, V.L. Dalal, G. Chumanov, and R. Bartels, "Low Temperature Epitaxial Silicon Growth Using High Vacuum Electron-Cyclotron-Resonance Plasma Deposition", *Appl. Phys. Lett.* 66, 2528-2530 (1995)
38. L. Breaux, B. Anthony, T. Hsu, S. Banerjee, and A. Tasch, "Homoepitaxial Films Grown on Si (100) at 150°C by remote plasma-enhanced chemical vapor deposition", *Appl. Phys. Lett.* 55, 1885-1887 (1989)
39. M.-D. Shieh, C. Lee, C.-H. Chen, T.-R. Yew, and C.-Y. Kung, "Low Temperature (313°C) Silicon Epitaxial Growth by Plasma-Enhanced Chemical Vapor Deposition with Stainless Steel Mesh", *Appl. Phys. Lett.* 63, 1252-1254 (1993)

40. C.C. Tsai, G.B. Anderson, and R. Thompson, "Low Temperature Growth of Epitaxial and Amorphous Silicon in a Hydrogen-Diluted Silane Plasma", in *14th Int. Conf. on Amorphous Semiconductors - Science and Technology* Garmisch-Partenkirchen, (1991)

41. C.-H. Chen, C.-M. Wan, and T.-R. Yew, "Silicon Epitaxial Growth at 300°C by Plasma Enhanced Chemical Vapor Deposition from SiH4/H2", *Appl. Phys. Lett.* **62**, 3126-3128 (1993)

42. C.-H. Chen and T.-R. Yew, "Silicon Epitaxial Growth by Plasma Enhanced Chemical Vapor Deposition from SiH4/H2 at 165-350°C", *J. of Crystal Growth* **147**, 305-312 (1995)

43. S. Veprek, F.A. Sarott, S. Rambert, and E. Taglauer, *J. Voc. Sci. Technol. A* **7**, 2614 (1989)

44. P. Torres, H. Keppner, R. Flückiger, J. Meier, and A. Shah, "Passivation of Crystalline Silicon Solar Cell Wafers by Amorphous and Microcrystalline Silicon Layers Deposited by VHF-GD", in *12th European Photovoltaic Solar Energy Conference* Amsterdam, 132-135 (1994)

45. M.A. Green and S.R. Wenham, "Novel Parallel Multijunction Solar Cell", *Appl. Phys. Lett.* **6S**, 2907-2909 (1994)

46. G. Willeke, "Physics and Electronic Properties of Microcrystalline Semiconductors", in *Amorphous & Microcrystalline Semiconductor Devices Vol. 2)*, edited by J. Kanicki (Artech House, Inc., 1992), pp. 55-87

47. G. Lucovsky, C. Wang, M.J. Williams, Y.L. Chen, and D.M. Maher, "Transport and Microstructure of Microcrystalline Silicon Alloys", *Mat. Res. Soc. Symp. Proc.* **283**, 443-454 (1993)

48. A. Poruba, Z. Remes, J. Fric, M. Vanecek, J. Meier, P. Torres, N. Beck, N. Wyrsch, and A. Shah, "Microcrystalline Silicon Thin Films Cells: Differences in the Cell and Material Properties", in *14 h European Photovoltaic Solar Energy Conference* Barcelona, 2105-2108 (1997)

49. M. Vanecek, A. Poruba, Z. Remes, N. Beck, and M. Nesladek, "Optical Properties of Microcrystalline Materials", *J. of Non-Cryst. Solids* **227-230**, 967-972 (1998)

50. A. Matsuda, "Formation Kinetics and Control of Microcrystallite in μc-Si:H from Glow Discharge Plasma", *J. of Non-Cryst. Solids* **59&60**, 767-774 (1983)

51. A. Matsuda, K. Kumagai, and K. Tanaka, "Wide-Range Control of Crystallite Size and Its Orientation in Glow-Discharge Deposited μc-Si:H", *Jpn. J. Appl. Phys.* **22**, L34-L36 (1983)

52. P.G. LeComber, "Some New Results on transport and Density of State Distribution in Glow Discharge Microcrystalline Silicon", *J. of Non-Cryst. Solids* **59&60**, 795-798 (1983)

53. J. Meier, S. Dubail, R. Flückiger, D. Fischer, H. Keppner, and A. Shah, "Intrinsic Microcrystalline Silicon (μc-Si:H) - A Promising new Thin Film Solar Cell Material", in *1st WCPEC* Hawaii, 409-412 (1994)

54. C. Wang and G. Lucovsky, "Intrinsic Microcrystalline Silicon (μc-Si:H) Deposited by Remote PECVD: A New Thin-Film Photovoltaic Material", in *21st IEEE Photovoltaic Specialists Conference* 2, Kissimimee, 1614-1618 (1990)

55. F. Wang, R. Schwarz, S. Grebner, H.N. Liu, Y.L. He, and C.Z. Liu, "Effect of Crystallinity on the Optoelectronics Properties of Hydrogenated Microcrystalline Silicon", in *Proc. of Int. Conf. of Phys. of Semicond., 21st ICPS* Beijing, 2008 (1992)

56. P. Torres, J. Meier, R. Flückiger, U. Kroll, J.A.A. Selvan, H. Keppner, A. Shah, S.D. Littlewood, I.E. Kelly, and P. Giannoulès, "Device Grade Microcrystalline Silicon Owing to Reduced Oxygen Contamination", *Appl. Phys. Lett.* 69, 1373-1375 (1996)

57. M.A. Green, *High Efficiency Silicon Solar Cells*, ed., Aedermannsdorf: Trans Tech SA, 1987, ISBN 0-87849-537-1

58. N. Beck, J. Meier, J. Fric, Z. Remes, A. Poruba, R. Flückiger, J. Pohl, A. Shah, and M. Vanecek, "Enhanced Optical Absorption in Microcrystalline Silicon", *J. of Non-Cryst. Solids* 198-200, 903-906 (1996)

59. N. Beck, "Optical and Electrical Properties of Hydrogenated Amorphous and Microcrystalline Silicon for Solar Cell Applications", *Ph. D. Thesis*, Institut de Microtechnique, University of Neuchâtel, Neuchâtel, 1997, ISBN 3-930803-26-7

60. W.E. Spear, G. Willeke, and P.G. LeComber, "Electronic Properties of Microcrystalline Silicon Prepared in the Glow Discharge Plasma", *Physica* **117B & 118B**, 908-913 (1983)

61. M.J. Williams, C. Wang, and G. Lucovsky, *J. of Non-Cryst. Solids* 137&138, 737 (1991)

62. G. Lucovsky, C. Wang, R.J. Nemanich, and M.J. Williams, "Deposition of μc-Si and μc-Si-C Thin Films by remote PECVD", *Solar Cells* 30, 419 - 434 (1991)

63. S.M. Cho, S.S. He, and G. Lucovsky, "Ambipolar Diffusion Lengths and Photoconductivity in B2H6 Doped μc-Si", in *Material Research Society Symposium Proceedings* San Francisco, (1994)

64. R. Flückiger, J. Meier, M. Goetz, and A. Shah, "Electrical Properties and Degradation Kinetics of Compensated Hydrogenated Microcrystalline Silicon Deposited by VHF-GD", *J. Appl. Phys.* 77, 712-716 (1995)

65. J. Meier, P. Torres, R. Platz, S. Dubail, U. Kroll, J.A.A. Selvan, N.P. Vaucher, C. Hof, D. Fischer, H. Keppner, A. Shah, K.-D. Ufert, P. Giannoulès, and J. Koehler, "On the Way towards High Efficiency Thin-Film Silicon Solar Cells by the "Micromorph" Concept", *Mat. Res. Soc. Symp. Proc.* 420, 3-14 (1996)

66. A.F. Fahrenbruch and R.H. Bube, *Fundamentals of Solar Cells, Photovoltaic Solar Energy Conversion*, ed., New York: I. Academic Press, 1983, ISBN 0-12-247680-8

67. S.M. Sze, *Physics of Semiconductor Devices*, 2 ed., I. John Wiley &Sons, 1981, ISBN 0-471-09837-X

68. S.M. Sze, *Semiconductor Devices, Physics and Technology*, ed. John Wiley & Sons, 1985, ISBN 0-471-83704-0

69. H.J. Möller, *Semiconductors for Solar Cells*, Artech House, 1993, ISBN 0-89006-574-8

70. S. Veprek, Z. Iqbal, R.O. Kühne, P. Capezzuto, F.-A. Sarott, and J.K. Gimzewski, "Properties of microcrystalline silicon: IV. Electrical conductivity, electron spin resonance and the effect of gas adsorption", *J. Phys. C: Solid State Phys.* **16**, 6241-6262 (1983)

71. U. Kroll, J. Meier, H. Keppner, A. Shah, S.D. Littlewood, I.E. Kelly, and P. Giannoulès, "Origins of Atmospheric Contamination in Amorphous Silicon Prepared by VHF-GD (70 MHz)", *J. Vac. Sci. Technol. A* **13**, 2742-2746 (1995)

72. U. Kroll, J. Meier, H. Keppner, S.D. Littlewood, I.E. Kelly, P. Giannoulès, and A. Shah, "Origin and Incorporation Mechanism for Oxygen Contaminants in a-Si:H and μc-Si:H Films prepared by the Very High Frequency (70 MHz) Glow Discharge Technique", *Mat. Res. Soc. Symp. Proc.* **377**, 39-44 (1995)

73. J.A.A. Selvan, H. Keppner, and A. Shah, "The Growth of Surface Textured Aluminium Doped ZnO Films for a-Si:H Solar Cells by RF-Magnetron Sputtering at Low Temperatures", *Mat. Res. Soc. Symp. Proc.* **426**, 497-502 (1996)

74. J.A.A. Selvan, "ZnO films for solar cell applications", *Ph. D. Thesis*, Institut de Microtechnique, University of Neuchâtel, Neuchâtel, 1998.

75. J. Meier, S. Dubail, J. Cuperus, U. Kroll, R. Platz, P. Torres, J.A.A. Selvan, P. Pernet, N. Beck, N.P. Vaucher, C. Hof, D. Fischer, H. Keppner, and A. Shah, "Recent Progress in Micromorph Solar Cells", *J. of Non-Crystalline Solids* **227-230**, 1250-1256 (1997)

76. J. Meier, H. Keppner, S. Dubail, U. Kroll, P. Torres, P. Pernet, Y. Ziegler, J.A.A. Selvan, J. Cuperus, D. Fischer, and A. Shah, "Microcrystalline Single-Junction And Micromorph Tandem Thin Film Silicon Solar Cells", to be publ. in *Material Research Society Symposium Proceedings* San Francisco, (1998)

77. J. Cifre, J. Bertomeu, J. Puigdollers, M.C. Polo, and J. Andreu, "Polycrystalline Silicon Films Optained By Hot-Wire Chemical Vapour Deposition", *Applied Physics* A S9, 645 (1994)

78. A.R. Middya, A. Lloret, J. Perrin, J. Huc, J.L. Moncel, J.Y. Parey, and G. Rose, "Fast Deposition of Photoconductive Polycrystalline Silicon by Hot-Wire CVD", *Mat. Res. Soc. Symp. Proc.* 377, 119 - 124 (1995)

79. J.K. Rath, K.F. Feenestra, D. Ruff, H. Meiling, and R.E.I. Schropp, "Purely Intrinsic Poly-Silicon Films by Hot-Wire CVD", *Mat. Res. Soc. Symp. Proc.* **452**, 977-982 (1997)

80. N. Wyrsch, N. Beck, J. Meier, P. Torres, and A. Shah, "Electric Field Profile in μc-Si:H p-i-n Devices", in *to be publ. in Proc. of MRS* San Francisco, (1998)

81. M. Goerlitzer, N. Beck, P. Torres, N. Wyrsch, and A. Shah, "Ambipolar Diffusion Length and Photoconductivity Measurements on "midgap" Hydrogenated Microcrystalline Silicon", *J. Appl. Phys.* **80**, 5111-5115 (1996)

82. A. Fejfar, N. Beck, H. Stuchlikova, N. Wyrsch, P. Torres, J. Meier, A. Shah, and J. Kocka, "On the Transport Properties of Microcrystalline Silicon", *J. of Non-Crystalline Solids* **227-230**, 227-230, (1997)

83. J. Merten, A. Munoz, C. Voz, J. Andreu, J. Meier, P. Torres, and A. Shah, "Variable Illumination Measurements of Microcrystalline Silicon solar Cells", in *14th European Photovoltaic Solar Energy Conference*, 1424-1426 Barcelona, (1997)

84. A. Shah, J. Meier, P. Torres, U. Kroll, D. Fischer, N. Beck, N. Wyrsch, and H. Keppner, "Recent Progress on Microcrystalline Silicon Solar Cells", in *26th IEEE Photovoltaic Specialists Conference* Anaheim (CA), 569-574 (1997)

85. M. Goerlitzer, P. Torres, N. Beck, N. Wyrsch, U. Kroll, H. Keppner, J. Pohl, and A. Shah, "Structural Properties and Electronic Transport in Intrinsic Microcrystalline Silicon Deposited by the VHF-GD Technique", *J. of Non-Crystalline Solids* **227-230**, 996-1000 (1997)

86. M. Goerlitzer, "Propriétées électroniques et structurels du silicium microcrystallin hydrogéné", *Ph. D. Thesis*, Institut de Microtechnique, University of Neuchâtel, Neuchâtel, 1998.

87. U. Kroll. private communication.

88. H. Shanks, C.J. Fang, L. Ley, M. Cardona, F.J. Demond, and S. Kalbitzer, *Phys. Status Solidi B* **110**, 43 (1980)

89. M.H. Brodsky, M. Cardona, and J.J. Cuomo, "Infrared and Raman spectra of the silicon-hydrogen bonds in amorphous silicon prepared by glow discharge and sputtering", *Physical Review B* **16**, 3556-3568 (1977)

90. A.A. Langford, M.L. Fleed, and M.H. Mahan, *Solar Cells* **27**, 373 (1989)

91. U. Kroll, J. Meier, A. Shah, S. Mikhailov, and J. Weber, "Hydrogen in Amorphous and Microcrystalline Silicon Films Prepared by Hydrogen Dilution", *J. Appl. Phys.* **80**, (1996)

92. H. Wagner and W. Beyer, "Reinterpretation of the Silicon-Hydrogen Stretch Frequencies in Amorphous Silicon", *Sol. State Comm.* **48**, 585-587 (1983)

93. Y.J. Chabal, E.E. Chaban, and S.B. Christman, "High Resolution Infrared Study of Hydrogen Chemisorbed on Si (100)", *J. Electron Spectr. and Rel. Phenom.* **29**, 35-40 (1983)

94. Y.C. Chabal, "Hydrogen Vibration on Si (111) 7x7: Evidence for a Unique Chemisorption Site", *Phys. Rev. Lett.* **50**, 1850-1853 (1983)

95. T. Satoh and A. Hiraki, "Detailed Study of Si-H Stretching Modes in μc-Si:H Film through Second Derivative IR Spectra", *Jpn. J. Appl. Phys.* **24**, 7, L491-L494 (1985)

96. M.A. Green and M.J. Keevers, "Optical Properties of Intrinsic Silicon at 300 K", *Pr. in PV: R. and Appl.* **1**, 189-192 (1995)

97. P. Torres, J. Meier, M. Goetz, N. Beck, U. Kroll, H. Keppner, and A. Shah, "Microcrystalline Silicon Solar Cells at Higher Deposition Rates by the VHF-GD", *Mat. Res. Soc. Symp. Proc.* **452**, 883-888 (1997)

98. M. Goetz, P. Torres, P. Pernet, J. Meier, D. Fischer, H. Keppner, and A. Shah, "n-i-p Micromorph Solar Cells On Aluminium Substrates", *Mat. Res. Soc. Symp. Proc.* **452**, 877-882 (1997)

99. N. Beck, P. Torres, J. Fric, Z. Remes, A. Poruba, H. Stuchlikova, A. Fejfar, N. Wyrsch, M. Vanecek, J. Kocka, and A. Shah, "Optical and Electrical Properties of Undoped Microcrystalline Silicon Deposited by the VHF-GD with Different Dilutions of Silane in Hydrogen", *Mat. Res. Soc. Symp. Proc.* **452**, 761-766 (1997)

100. K. Köhler, D.E. Horne, and J.W. Coburn, *J. Appl. Phys.* **58**, 3350 (1985)

101. P. Hapke, "VHF-Plasmaabscheidung von mikrokristallinem Silizium (μc-Si:H): Einfluss der Plasmaanregungsfrequenz auf die strukturellen und elektrischen Eigenschaften", *Ph. D. Thesis*, Technical University Aachen, 1995.

102. W.B. Jackson, N.M. Johnson, and D.K. Biegelsen, *Appl. Phys. Lett.* **43**, 195 (1983)

103. P. Torres, J. Meier, U. Kroll, N. Beck, H. Keppner, and A. Shah, "Fast Deposited Microcrystalline Silicon Solar Cells", in *26th IEEE Photovoltaic Specialists Conference* Anaheim, CA, 711-714 (1997)

104. P. Torres, H. Keppner, J. Meier, U. Kroll, N. Beck, and A. Shah, "Fast Deposition of μc-Si:H by Restrictive Dilution and Enhanced HF-power", *Physica Status Solidi (a); Rapid Research Notes* **163/2**, R9 (1997)

105. A. Poruba, "Constant Photocurrent Method - Study of Optical Properties of Amorphous Hydrogenated Silicon Prepared by Microwave Plasmas", *Ph. D. Thesis*, Faculty of Chemistry, Technical University of Brno, Brno, 1998.

106. P. Pernet, M. Goetz, H. Keppner, and A. Shah, "Growth of Thin <p> μc-Si:H on Intrinsic a-Si:H for <nip> Solar Cells Application", *Mat. Res. Soc. Symp. Proc.* **452**, 889-894 (1997)

107. N. Beck, N. Wyrsch, C. Hof, and A. Shah, "Mobility Lifetime Products - A Tool for Correlating a-Si:H Film Properties and Solar Cell Performances", *J. Appl. Phys.* **79**, 9361-9368 (1996)

108. A. Shah et al., "unpublished data"

109. M.J. Kushner, "A model for the discharge kinetics and plasma chemistry during plasma enhanced chemical depositioo of amorphous silicon", *J. Appl. Phys.* 63 (8), 2532-2551 (1988)

110. Y. Mishima, S. Miyazaki, M. Hirose, and Y. Osaka, "Characterisation of Plasma-Deposited Microcrystalline Silicon", *Phil. Mag. B* **46**, 1-12 (1982)

111. S. Oda, J.I. Noda, and M. Matsumura, "Preparation of a-Si:H Films by VHF Plasma CVD", in *Amorphous Silicon Technology* **118**, Reno, Nevada, 117-122 (1988)

112. S. Oda, J.I. Noda, and M. Matsumura, "Diagnostic Study of VHF Plasma and Deposition of Hydrogenated Amorphous Silicon Films", *Jpn. J. Appl. Phys.* **29**, 1889-1895 (1990)

113. P. Torres, U. Kroll, H. Keppner, J. Meier, E. Sauvain, and A. Shah, "Deposition of Thin-Film Silicon for Photovoltaics: Use of VHF-GD and OES", to *be published in Proc. of the 5th Thermal Plasma Processes* St. Petersburg, (1998)

114. M. Otobe and S. Oda, "The Role of Hydrogen Radicals in the Nanocrystallization of Silicon", *Proc. Jpn. Plasma Chem.* **5**, 123-128 (1992)

ACKNOWLEDGMENTS

I would like to thank:

Professor A. Shah who spontaneously accepted me in his dynamic research group; for giving me the freedom and confidence to develop my own ideas through all the past years. His expert guidance has had an immanent scientific impact to this present work.

My friends and mentors Hannes Meier, Ulli Kroll and Herbert Keppner, who always encouraged me in difficult moments to "dig further" and coovinced me in those difficult moments not to send my reactor vessel to the bottom of the lake of Neuchâtel. I especially appreciated the open, critical and stimulating scientific and sometimes also philosophical discussions we had together: their positive approach to experimental physics constantly helped me to overcome the apparently invincible technological limitations encountered.

Roger Flückiger who introduced me to the "tricky" technology and art of μc-Si:H deposition. I especially appreciated his sincere friendship and the nice time we spent together. I am most confident that the μc-Si:H "flame" that I got from him will further bum and grow in the hands of my successor Luc Feitknecht.

Michael Götz who introduced me to the upside down world of n-i-p solar cells. I especially admire his commitment to all sustainable forms of alternative energies.

Evelyne Vallat-Sauvain to have accepted to read entirely and meticulously this manuscript to render it understandable and for the "private lessons" in crystallography.

All my colleagues and friends from the "Thin-Film Silicon" group. By their constant encouragement and availability for help and discussions they have to a large extend contributed to this work.

Special thanks to Milan Vanecek, Ales Poruba and Zdenek Remes (Academy of Sciences of the Czech Republic) for not only patiently explaining me CPM-spectra, but also for the unforgettable nice time we spent together. I particularly appreciated their ability to extract, or to say in other words "distillate" the data that were most important for my further research.

Dr. U. Mallang, Dr. J. Köhler and Dr. J. Pohl from Konstanz University who freely accepted to perform X-ray measurements.

Dr. V. Vorlicek from the Academy of Sciences of the Czech Republic for performing Raman-spectra.

Prof. M. A. Green who immediately accepted me for a half year stay within his research group at the Photovoltaics Centre of UNSW (Sydney) and the Charles-Edouard Guillaume foundation for the provided financial support.

Prof. J. Andreu, Prof. N. deRooij, Dr. P. Seitz, Dr. A. A. Howling and Dr. H. Keppner who have spontaneously accepted to join the examination board and who have devoted their time to the lecture of this thesis.

My parents who unconditionally supported me to follow higher studies. For allowing me to follow up my interests and for the given freedom to let me choose to study physics instead of music.

Very, very special thanks to you, Natalie, for the endless moral support, for believing in this "poem-project" and for so many other things.

Aktuelle Titel Physik

Band 327: Beck, Natalie »Optical and electrical properties of hydrogenated amorphous and microcrystalline silicon for solar cell applications«
ISBN 3-930803-26-7, 112 Seiten, DM 78,–

Band 329: Schön, Jan Hendrik »Anwendungen von $CuGaSe_2$ in der Photovoltaik: Materialcharakterisierung und Solarzellenherstellung«
ISBN 3-930803-28-3, 164 Seiten, DM 85,–

Band 331: Käfer, Wolfgang »Neue Materialien für Peltier-Kühler: Das System $Mn^{IV}NiSn$ und andere Verbindungen«
ISBN 3-930803-30-5, 120 Seiten, DM 89,–

Band 335: Klewitz, Steffen »Stimulierte Lichtstreuung mit Besselstrahlen«
ISBN 3-930803-34-8, 186 Seiten, DM 89,–

Band 338: Filleböck, Georg »Selbstorganisierte Nanostrukturen: Diffusion und Agglomeration von Adatomen auf der anisotropen Pd(110)-Oberfläche«
ISBN 3-930803-35-6, 78 Seiten, DM 84,–

Band 339: Zimmermann, Stefan »Optische Eigenschaften elektrisch abstimmbarer lateraler Potentialübergitter in Halbleiterheterostrukturen«
ISBN 3-930803-38-0, 106 Seiten, DM 89,–

Band 340: Koch, Uwe »Architekturunabhängiges Checkpointing paralleler Anwendungen am Beispiel von Monte-Carlo-Simulationen der Emission eines Röntgenpulsars«
ISBN 3-930803-39-9, 146 Seiten, DM 89,–

Band 341: Storz, Rafael »Frequenzstabilisierung von Festkörperlasern auf makroskopische und mikroskopische Frequenzen«
ISBN 3-930803-40-2, 122 Seiten, DM 89,–

Band 344: Nowak, Stephan »Atomoptische Interferenz- und Lithographieexperimente mit metastabilem Helium«
ISBN 3-930803-43-7, 148 Seiten, DM 89,–

Band 349: Breitenbach, Gerd »Quantum state reconstruction of classical and nonclassical light and a cryogenic opto-mechanical sensor for high-precision interferometry«
ISBN 3-930803-48-8, 146 Seiten, DM 89,–

Band 350: Rettenberger, Armin »Selbstorganisiertes Wachstum metallischer Nanostrukturen auf Schichtgitterhalbleitern«
ISBN 3-930803-49-6, 136 Seiten, DM 89,–

Band 354: Neser, Stephan »Kolloidale Kristalle in eingeschränkter Geometrie«
ISBN 3-930803-53-4, 152 Seiten, DM 89,–

Band 355: Ernst, Urban »Bose-Einstein-Kondensation von Rubidiumatomen«
ISBN 3-930803-54-2, 138 Seiten, DM 89,–

Band 357: Hofer, Anselm »Niederenergetische Myonen: Eigenschaften und Anwendungen«
ISBN 3-930803-56-9, 164 Seiten, DM 89,–

Band 359: Spiegel, Markus »Microwave induced remote hydrogen plasma (MIRHP) passivation of multicrystalline silicon solar cells«
ISBN 3-930803-58-5, 140 Seiten, DM 89,–

UFO Atelier für Gestaltung & Verlag · E.-Mühlenweg-Str. 12 · 78478 Allensbach
Telefon 07533/971966 · Fax 07533/971967 · Internet http://www.ufo.xnet.de